NAVAL POSTGRADUATE SCHOOL

MONTEREY, CALIFORNIA

THESIS

COLD SPRAY SURFACE PATTERNING OF ALUMINUM ON ALUMINUM, SILICON, GLASS, AND PRINTED CIRCUIT BOARD SUBSTRATES

by

Jonathan E. Palao

December 2017

Thesis Advisor: Chun-Hsien Wu
Second Reader: Joe Hooper

Approved for public release. Distribution is unlimited.

THIS PAGE INTENTIONALLY LEFT BLANK

REPORT DOCUMENTATION PAGE			Form Approved OMB No. 0704-0188

1. AGENCY USE ONLY *(Leave blank)*	2. REPORT DATE December 2017	3. REPORT TYPE AND DATES COVERED Master's thesis

4. TITLE AND SUBTITLE COLD SPRAY SURFACE PATTERNING OF ALUMINUM ON ALUMINUM, SILICON, GLASS, AND PRINTED CIRCUIT BOARD SUBSTRATES	5. FUNDING NUMBERS
6. AUTHOR(S) Jonathan E. Palao	
7. PERFORMING ORGANIZATION NAME(S) AND ADDRESS(ES) Naval Postgraduate School Monterey, CA 93943-5000	8. PERFORMING ORGANIZATION REPORT NUMBER
9. SPONSORING /MONITORING AGENCY NAME(S) AND ADDRESS(ES) N/A	10. SPONSORING / MONITORING AGENCY REPORT NUMBER

11. SUPPLEMENTARY NOTES The views expressed in this thesis are those of the author and do not reflect the official policy or position of the Department of Defense or the U.S. Government. IRB number ____N/A____.

12a. DISTRIBUTION / AVAILABILITY STATEMENT Approved for public release. Distribution is unlimited.	12b. DISTRIBUTION CODE

13. ABSTRACT (maximum 200 words)

The aim of the present study is to investigate the feasibility of and the criteria for using the cold spray technique for surface patterning to create two-dimensional surface features on various substrates. Metal meshes were used as screens for surface patterning in this investigation; fabricated features were characterized with optical microscope, scanning electron microscope, and optical profilometer. Processing parameters like mesh size, standoff distance, gun traverse speed, and number of spray passes were examined to study their influence on the morphology of the fabricated features. Two-dimensional aluminum features were successfully fabricated on aluminum, soda-lime glass, silicon wafer, and the copper foil-layer of printed circuit board. The smallest feature, created with -45 to +5 μm aluminum feedstock powders, has an average size of 67.4 μm. It was determined that the pore size of a mesh needs to be at least 3.3 times bigger than the average size of feedstock powders in order to create features successfully. To estimate the probability of feedstock powders passing through a mesh and simulate the topography of the fabricated features, a Monte Carlo simulation incorporating the particles' size distribution and the geometry meshes was developed. With the capability of creating features on diverse substrates, the cold spray surface patterning technique shows promising potential to create heterogeneous two-dimensional functional features or devices at micron size with high efficiency.

14. SUBJECT TERMS cold spray, surface patterning, surface modification, functional coating	15. NUMBER OF PAGES 73
	16. PRICE CODE

17. SECURITY CLASSIFICATION OF REPORT	18. SECURITY CLASSIFICATION OF THIS PAGE	19. SECURITY CLASSIFICATION OF ABSTRACT	20. LIMITATION OF ABSTRACT
Unclassified	Unclassified	Unclassified	UU

NSN 7540-01-280-5500 Standard Form 298 (Rev. 2-89)
Prescribed by ANSI Std. 239-18

THIS PAGE INTENTIONALLY LEFT BLANK

Approved for public release. Distribution is unlimited.

COLD SPRAY SURFACE PATTERNING OF ALUMINUM ON ALUMINUM, SILICON, GLASS, AND PRINTED CIRCUIT BOARD SUBSTRATES

Jonathan E. Palao
Lieutenant Commander, Peruvian Navy
B.S., Peruvian Naval Academy, 2004

Submitted in partial fulfillment of the
requirements for the degree of

MASTER OF SCIENCE IN MECHANICAL ENGINEERING

from the

NAVAL POSTGRADUATE SCHOOL
December 2017

Approved by: Chun-Hsien Wu
Thesis Advisor

Joe Hooper
Second Reader

Garth V. Hobson
Chair, Department of Mechanical and Aerospace Engineering

THIS PAGE INTENTIONALLY LEFT BLANK

ABSTRACT

The aim of the present study is to investigate the feasibility of and the criteria for using the cold spray technique for surface patterning to create two-dimensional surface features on various substrates. Metal meshes were used as screens for surface patterning in this investigation; fabricated features were characterized with optical microscope, scanning electron microscope, and optical profilometer. Processing parameters like mesh size, standoff distance, gun traverse speed, and number of spray passes were examined to study their influence on the morphology of the fabricated features. Two-dimensional aluminum features were successfully fabricated on aluminum, soda-lime glass, silicon wafer, and the copper foil-layer of printed circuit board. The smallest feature, created with -45 to +5 μm aluminum feedstock powders, has an average size of 67.4 μm. It was determined that the pore size of a mesh needs to be at least 3.3 times bigger than the average size of feedstock powders in order to create features successfully. To estimate the probability of feedstock powders passing through a mesh and simulate the topography of the fabricated features, a Monte Carlo simulation incorporating the particles' size distribution and the geometry meshes was developed. With the capability of creating features on diverse substrates, the cold spray surface patterning technique shows promising potential to create heterogeneous two-dimensional functional features or devices at micron size with high efficiency.

THIS PAGE INTENTIONALLY LEFT BLANK

TABLE OF CONTENTS

I. INTRODUCTION 1
A. MOTIVATION 1
B. LITERATURE REVIEW ON COLD SPRAY 3
1. Cold Spray Deposition Process 3
2. Cold Spray Process Standoff Distance Influence 6
3. Cold Spray Bonding Mechanism 7
C. OBJECTIVES 8

II. EXPERIMENTAL PROCEDURES 11
A. FEEDSTOCK POWDERS 11
B. POWDER AND COATINGS CHARACTERIZATION 11
1. Particle Size Analysis 11
2. Preparation of Al Powder and Coating Samples 11
3. Scanning Electron Microscopy for Powder and Coatings 12
4. X-ray Diffraction 12
C. COATING PRODUCTION 13
1. Masked Cold Spray Deposition Experiments 15

III. RESULTS AND DISCUSSION 19
A. POWDER CHARACTERISTICS 19
1. Particle Sizing 19
2. Particle Morphology 20
3. X-ray Diffraction 21
B. COLD-SPRAY COATINGS 21
1. Masks and Substrates 21
2. Pore and Feature Size 24
3. Monte Carlo Simulation 31
4. Standoff Distance between Mesh and Substrate 35
5. Gun Traverse Speed and Number of Passes 40

IV. CONCLUSION 45

LIST OF REFERENCES 47

INITIAL DISTRIBUTION LIST 53

THIS PAGE INTENTIONALLY LEFT BLANK

LIST OF FIGURES

Figure 1. Standard schematic diagram of cold-gas dynamic spray system. Source: [36]. 4

Figure 2. SEM of copper particles on copper substrate. Source: [33]. 4

Figure 3. Particle velocity versus gas temperature for various spray methods. Source: [35]. 5

Figure 4. Cross-sectional view of aluminum coating on glass substrate. 5

Figure 5. Schematic diagram of the supersonic impingement zone at the substrate. Source: [39]. 7

Figure 6. Impact of copper particle on copper substrate at successive times. Source: [40]. 7

Figure 7. The schematic view of different region of particles on substrate. Source: [41]. 8

Figure 8. Centerline SST Model Series C low-pressure cold spray system installed at the Naval Postgraduate School. 14

Figure 9. 3D printed ABS mesh (a) as received, and (b) deformed. 15

Figure 10. SEM images showing pore and wire size (a) 16, (b) 45, (c) 170, (d) 200, and (e) 400. 16

Figure 11. Particle size distribution for the SST-A5001 aluminum powder. 19

Figure 12. Inlens SEM images of the SST-A5001 aluminum powder (a) 400X, and (b) 20kX Mag. 20

Figure 13. Backscatter detector cross-section images of the SST-A5001 aluminum powder showing their grain structure. 20

Figure 14. XRD pattern of SST-A5001 Al powder. 21

Figure 15. Non-conductive side of PCB (a) surface erosion, and (b) grooves formation. 22

Figure 16. Two-dimensional features fabricated on (a) aluminum, (b) silicon wafer, (c) glass, and (d) copper foil layer of PCB with cold spray surface patterning technique. 23

Figure 17. SEM images show the morphology of (a) mesh 16, (b) mesh 170, and (c) mesh 200; the morphology of the features fabricated with (d) mesh 16, (e) mesh 170, and (f) mesh 200; the topography of the feature fabricated with (g) mesh 16. Line profiles of the feature heights of features fabricated with mesh 170 and mesh 200 obtained by optical profilometer are shown in (h) and (i), respectively. 26

Figure 18. Size distribution of features fabricated with mesh 200 and pore size of mesh 200. The diamond shows the 95% confidence intervals of individual data set and one-way analysis of variance data. 28

Figure 19. (a) Optical image of cold sprayed coating at a single location with duration of 200 seconds. (b) Schematic drawing of the recirculation zone near the edges of a screen (not to scale). 29

Figure 20. SEM images of aluminum cold sprayed features fabricated with (a) mesh 16 and (b) mesh 45 on a copper foil layer of PCB. 31

Figure 21. SEM images of aluminum cold sprayed features fabricated with (a) mesh 16 and (b) mesh 45 on silicon wafer substrate. 31

Figure 22. Simulated features of (a) mesh 170, (b) mesh 200, and (c) mesh 400 by Monte Carlo simulation with 25,000 particles and experimental particle size distribution measured by laser scattering analysis. Successful bonding of particles to the substrates was limited to feedstock powders with particle size of 10 μm and above. The corresponding line profiles of the vertical center features in (a), (b), and (c) are shown in (d), (e), and (f). 33

Figure 23. The feature heights versus the standoff distances between meshes and substrates of the five paired data sets fabricated with standoff distances of 0mm, 1mm, 1.7mm, 2.37mm, and 3.7mm on PCB and silicon substrates. 36

Figure 24. The samples PCB-5 and PCB-6, fabricated with 0 mm and 1.7 mm standoff distances, are shown in (a) and (b); the samples PCB-7 and PCB-2, fabricated with 0 mm and 1.7 mm standoff distances, are shown in (c) and (d); the samples PCB-3 and PCB-4, fabricated with 1.7 mm and 3.7 mm standoff distances, are shown in (e) and (f). Note: the samples listed here represent the data shown in Figure 23. 38

Figure 25. The samples Si-5 and Si-6, fabricated with 0 mm and 2.37 mm standoff distances, are shown in (a) and (b); the samples Si-3 and Si-4, fabricated with 1 mm and 2.37 mm standoff distances, are shown in 25 (c) and (d). Note: the samples listed here represent the data shown in Figure 23. 39

Figure 26. Optical Images and SEM images of aluminum features fabricated with mesh 16 and gun traverse speeds of (a) 10 mm/s, and (b) 20 mm/s, with mesh 45 and gun traverse speed of (c) 20 mm/s, and (d) 40 mm/s. 41

Figure 27. SEM images of aluminum features fabricated with (a) one pass and (b) two passes. 43

THIS PAGE INTENTIONALLY LEFT BLANK

LIST OF TABLES

Table 1. Dimensions of de Laval nozzle used in experiments. 14

Table 2. Pore size and wire size of meshes 60, 45, 170, 200, and 400. 16

Table 3. Cold spray parameters utilized on masked PCB substrates. 16

Table 4. Cold spray parameters utilized on masked silicon wafer substrates. 17

Table 5. Cold spray parameters utilized on masked aluminum substrates. 17

Table 6. SST-A5001 aluminum powder, particle size characteristics. 19

Table 7. Cold spray processing parameters and height of features fabricated with meshes (16, 170, 200, and 400), on aluminum substrate. 23

Table 8. Cold spray processing parameters and height of features fabricated with meshes 16, 45, and 5/16” on glass and silicon wafer substrates. 24

Table 9. Cold spray processing parameters and height of features fabricated with meshes 16 and 45 on copper foil layers of PCB. 24

Table 10. Sample IDs, pore and wire size of meshes (60, 170, and 400), feature size and height of the patterns fabricated on aluminum substrate. 25

THIS PAGE INTENTIONALLY LEFT BLANK

LIST OF ACRONYMS AND ABBREVIATIONS

ABS	Acrylonitrile Butadiene Styrene
Al	Aluminum
BSD	Back scatter detector
CGDS	Cold Gas Dynamic Spray
CS	Cold Spray
DE	Deposition efficiency
EDS	Energy Dispersive Spectroscopy
FCC	Face Centered Cubic
He	Helium
N2	Diatomic Nitrogen
NPS	Naval Postgraduate School
Mg	Magnesium
PCB	Printed Circuit Board
PMC	Polymer Matrix Composite
SE	Secondary Electron
SEM	Scanning Electron Microscopy
SST	Supersonic Spray Technologies
XRD	X-ray Diffraction

THIS PAGE INTENTIONALLY LEFT BLANK

ACKNOWLEDGMENTS

I would like to thank the Peruvian Navy for providing me with the opportunity to fulfill one of the most challenging goals that I have ever had. Studying at this distinguished academic institution is truly a once-in-a-lifetime opportunity and I feel deeply grateful for that.

Likewise, I am grateful to Dr. Chun-Hsien Wu for his guidance, generous assistance, and professionalism. Your positive attitude and passion for engineering and investigation is something that I am certainly going to remember. I would not have been able to accomplish this research without your help and support through this project.

I would also like to extend my gratitude to Professor Francesca Nice of the International Graduate Program at the Naval Postgraduate School. I could not have written coherent publications without her patience and constant willingness to help.

Last, but certainly not least, I would like to express my gratitude to my family for their constant support and encouragement throughout my entire career, and especially during the completion of this master's degree program.

THIS PAGE INTENTIONALLY LEFT BLANK

I. INTRODUCTION

A. MOTIVATION

Some of the most widely known surface-patterning techniques for preparing and creating patterns on surfaces, from the arrangement of a single atom to the macro-scale features include etching, laser patterning, lithography, and film deposition [1]–[8]. The first three techniques are commonly used to pattern surfaces by removal of materials [2]–[8]. Film deposition categories physical vapor deposition and chemical vapor deposition require systems under vacuum, and the surface area to be patterned is typically limited by the space of the system chamber [3], [9], [10].

Cold spray is a surface-coating technique, which is commonly used to produce: wear resistant, corrosion resistant, thermal barrier, anti-fouling, and conductive/nonconductive (electrical and thermal) coatings [11]–[18]. CS does not require vacuum and has high deposition efficiency, making possible to fabricate a coating of hundreds of microns thick on a square inch area within a few seconds. Moreover, some Cold spray systems are portable to be used in field. In 2011, DeForce et al. studied the utilization of CS to deposit a custom-made high-purity Al-5wt% Mg corrosion-resistant barrier coating on ZE41A-T5 Mg substrate. Findings showed that the produced coating was significantly harder than the substrate, had a strong adhesion and was galvanically compatible [19].

Cold spray is also used to restore expensive damaged parts and return them to a functional condition instead of being replaced, which is known as additive repairing [20]. Several authors have demonstrated the utility of CS on this application, for instance a corroded gearbox of a Seahawk helicopter was restored by cold spray, which provided cost savings of 35%–50% [21]. In addition to repairing capability, cold spray is also known for its potential in additive manufacturing [22]. Recently, M. E. Lynch et al. have demonstrated a designing

and optimizing process for cold spray additive manufacturing for a part with 20% reduction in weight [23]. In 2009, P. F. Leyman and V. K. Champagne deposited a highly adherent, dense aluminum composite material to repair a corroded 7075-T73 aluminum mast support on an Army helicopter; the deposited material was machined to dimensionally restore the component to its original condition. Adhesion, fatigue, and corrosion tests were conducted to evaluate the coating with favorable conclusive results [24].

Cold spray applications have extended beyond military field and got into medical field. A study conducted by the Department of Orthopedic Surgery at the Nara Medical University in Kashihara, Japan deposited the inorganic antimicrobial Novaron (grade VZ 600) on a titanium alloy surface and discovered that when the pressure of the carrier gas was increased, the coating adhered adequately showing good effects against infectious organisms [25].

Cold spray constitutes an efficient, cost effective, and environmentally friendly alternative to traditional methods. It also improves material properties and provides solution to temperature sensitive cases. All the applications of this technique described above, focus on fabrication of functional coatings, additive repairing, and additive manufacturing; however, the potential use of cold spray as a surface patterning technique was rarely investigated.

By incorporating a screen in cold spray process, bottom-up surface patterns can be generated. D. Kim et al. used cold spray to deposit one-dimensional copper lines with widths varying from 150 to 1500 μm on silicon wafer and soda-lime glass to explore the potential of cold spray technology to print electrodes in solar cell applications [13]. S. V. Klinkov et al. studied cold spray through a mask (wire) with transverse size in the range 0.3–1 mm to produce one-dimensional non-conductive path (region with no coating) [26]. Y. Cormier et al. explored the manufacturability of two dimensional fin arrays from 12 to 30 fins/in to serve as compact heat exchanger by cold spray process using steel wire mesh [27]–[29].

The prior publications focused on the production of one-dimensional features and the heat exchanging application of cold sprayed fins. The current study focuses on the fabrication of two-dimensional surface patterns through metal screens (meshes) to explore the influence of feedstock powders' particle size, meshes' pore and wire size, standoff distance, gun temperature, gun pressure, and gun traverse speed to the geometries of the patterned features on various substrates.

B. LITERATURE REVIEW ON COLD SPRAY

1. Cold Spray Deposition Process

Cold gas dynamic spray is a solid state coating technique. The feedstock powders are injected into a convergent-divergent (de Laval) nozzle and accelerated by high pressure gas (most commonly compressed air, nitrogen, and helium) to supersonic speeds (200 to 1200 m/s) [30]–[32]. A diagram of a standard low-pressure cold-spray system is shown in Figure 1. Once the impact velocities of the feedstock powders exceed a critical velocity [30], [33], [34], instead of bouncing back from a substrate the powders adhere to the substrate with plastic deformation (Figure 2).

This coating technique was first developed by professor A. Papyrin and his colleagues while studying different models in a wind tunnel, where the models were subjected to a supersonic flow constituted by gas and solid particles. During this experiment, a broad range of materials, such as metal alloys and composites, were successfully deposited onto a diverse types of substrates. After the publication of these original findings, this technique has been studied extensively and is currently used in several applications, from medical prostheses to engineering components reparation [35].

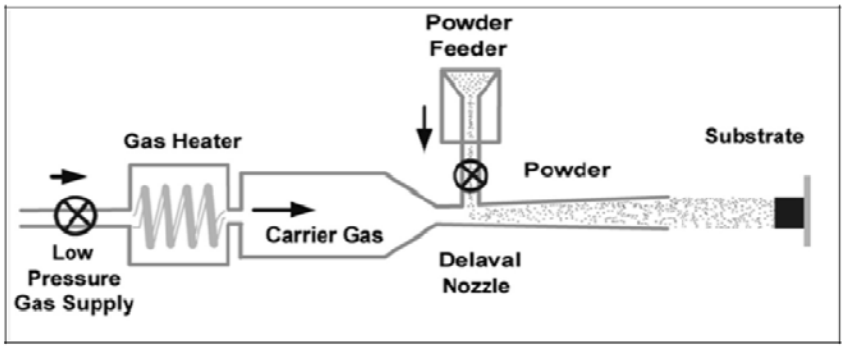

Figure 1. Standard schematic diagram of cold-gas dynamic spray system. Source: [36].

Cold spray is one of the different types of thermal spray processes that are commonly used to apply metallic coatings or add materials to restore corroded or damaged parts. The capability of depositing thick coatings at high deposition rates, is one of the most important advantages that can be obtained when using plasma, and flame spray; these techniques offer the possibility of using various feedstock materials and a wide range of substrates to be coated [35]. However, the coatings produced with these techniques could exhibit the formation of oxides and high levels of porosity [35]. A major difference and disadvantage compared to cold spray is that these techniques heat the feedstock powders above their melting point, which ultimately could alter the microstructure and mechanical properties of the coating and the substrate. [35].

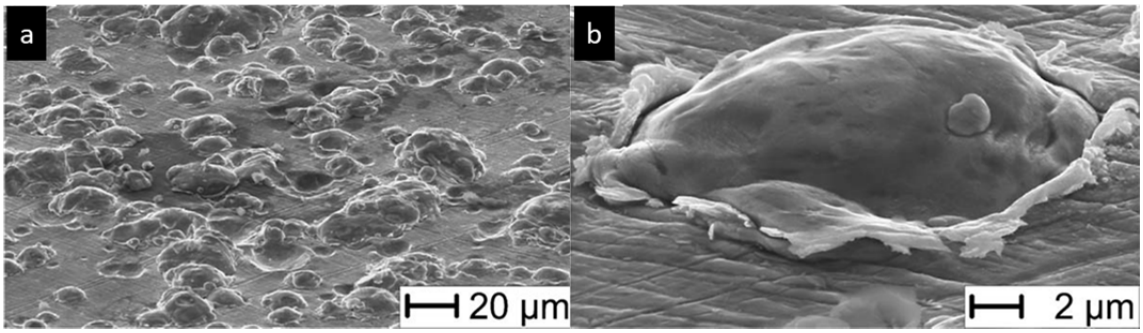

Substrate is shown in (a) an overview and (b) a close-up image.

Figure 2. SEM of copper particles on copper substrate. Source: [33].

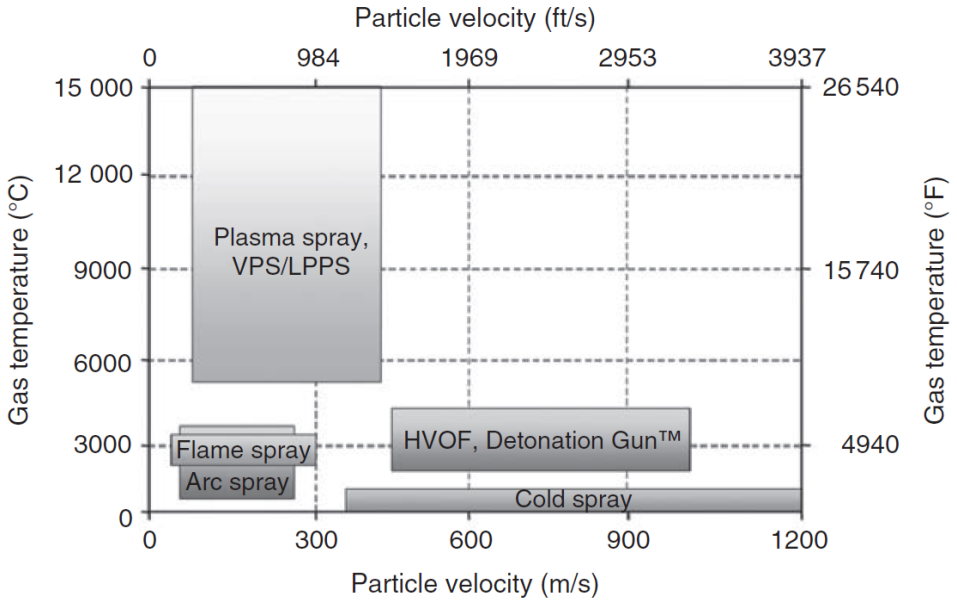

Figure 3. Particle velocity versus gas temperature for various spray methods. Source: [35].

As seen in Figure 3, compared with the other spray techniques, cold spray is performed at higher velocities and at a relatively low temperature. These particularities of cold spray do not create a heat-affected zone in the substrate, allow a denser coating, exhibit a porosity commonly below 1%, and result in a high deposition efficiency (Figure 4).

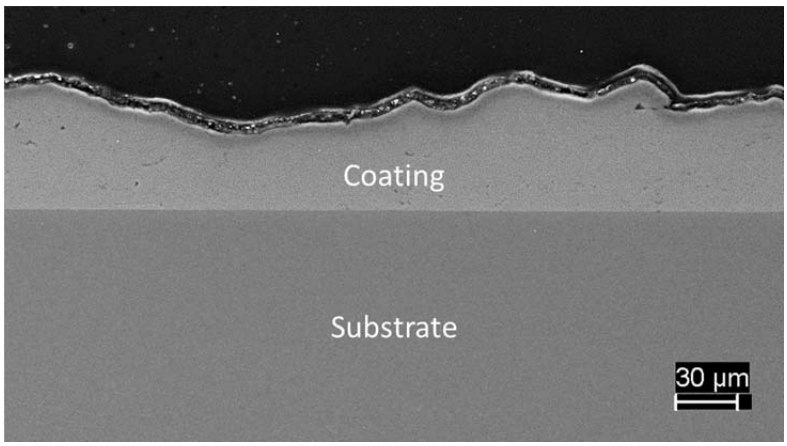

Figure 4. Cross-sectional view of aluminum coating on glass substrate.

The denser coating is due to the absence of splashing, which is a common outcome obtained when using thermal spray. Cold spray deposits the powder feedstock at supersonic speed. The impacting powders deform the previously deposited layer, close gaps, and, therefore, the coating porosity is reduced [6]. Assadi et al. suggested that thermal softening and adiabatic shear instability at the interface of particle and substrate plays an important role in bonding formation of cold spray [33], [37], [38].

Besides the benefit of low processing temperature, coatings of various materials: metals, metal matrix composites, ceramics, polymers, and nanomaterials can be fabricated with cold gas dynamic spray on various substrates: metals, ceramics, semiconductors, and polymers [11]–[13]. One of the most important and convenient advantage of this technique is that cold-spray coatings can be applied in field, because some of the systems are designed to be portable units.

2. Cold Spray Process Standoff Distance Influence

The standoff distance (SoD) from the nozzle to the substrate, can drastically affect the deposition of the particles. In [39], Pattison identifies that if the SoD is too short, a bow shock is formed at the impingement zone between the supersonic jet and the substrate (Figure 5), which is detrimental to the performance of the deposition process as it not only reduces the velocity of the gas below the critical velocity, but also the impacting velocity of the particles can be decreased. Pattison's study points out that at large SoD, when the bow shock is not present, deposition can continue without any impediment, but if the SoD is too large, drag due to air resistance could slow the particles below the critical velocity needed for deposition. He also concluded that deposition efficiency demonstrated to be directly related to SoD as a result of the formed bow shock and the relative velocity between the gas and the particles. The bow shock is related to the length of the supersonic core of the gas jet and is inversely

proportional to the SoD; however, it only becomes an issue at relatively close SoD (< 5 mm) [39].

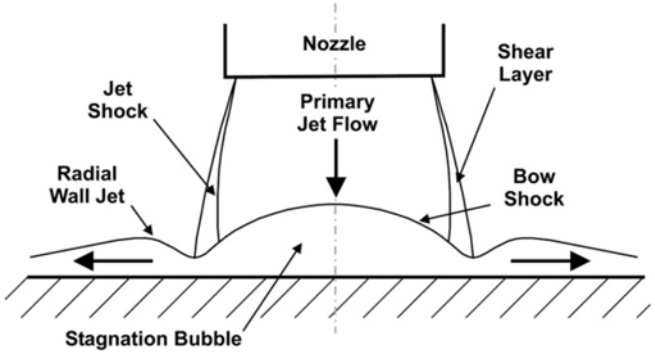

Figure 5. Schematic diagram of the supersonic impingement zone at the substrate. Source: [39].

3. Cold Spray Bonding Mechanism

Because of its particular characteristics, many studies have been performed to understand how the cold-spray bonding mechanism occurs. The adhesion is based on the severe plastic deformation of the powder particle on the substrate during the supersonic impact. In [40], Victor K. Champagne discusses that the bonding mechanism between the various layers created was due to the particles penetration onto the substrate, interfacial heating, and the supersonic velocity impact that leads to the liquid jet formation. These phenomena are depicted in Figure 6.

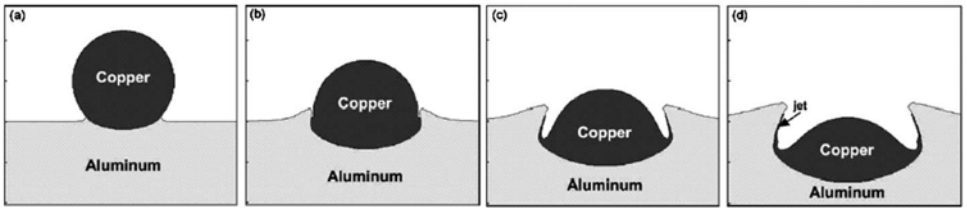

Elapsed times after impact are (a) 5 ns, (b) 20 ns, (c) 35 ns, and (d) 50 ns.

Figure 6. Impact of copper particle on copper substrate at successive times. Source: [40].

Due to its particular nature, measuring the deposition efficiency results a complicated task when using the cold-gas dynamic spray technique. To understand the deposition process, it was divided into four main stages as shown in Figure 7. Stage 1 is the impact area where a first particles impact directly onto the substrate causing erosion and bonding of the first layer of particles. Stage 2 is where particle deformation and realignment of the inbound particles occurs when they hit the already existing particle layer from stage 1. During stage 3 is produced the metallurgical bonding and void reduction of the incoming particles. Stage 4 is where bulk deformation (cracking, work hardening of particles, and removal of previously bonded particles) occurs and where an excess of kinetic energy is required [41].

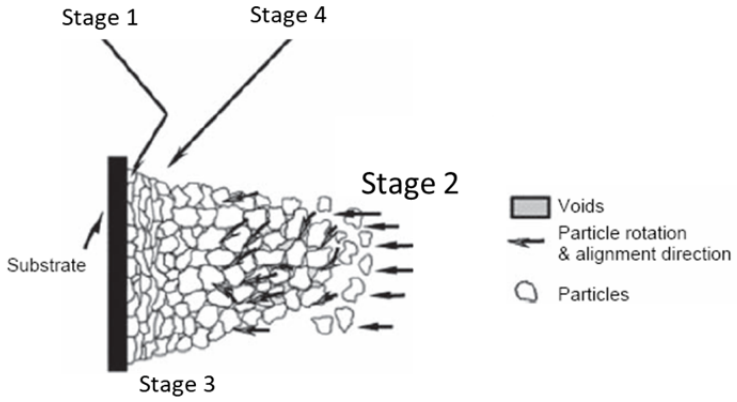

Figure 7. The schematic view of different region of particles on substrate. Source: [41].

C. OBJECTIVES

This thesis is organized and divided into five main technical objectives:

- Characterize the feedstock aluminum powder using laser scattering particle size analysis, scanning electron microscope (SEM), optical microscopy, and X-ray diffraction (XRD) to determine its suitability to be used in cold-spray surface patterning technique.
- Estimate the probability of feedstock powders passing through a mesh and to deposit onto the substrates' surfaces using a Monte

Carlo simulation, where particle size distribution and the geometry of the meshes were incorporated.

- Examine how the cold-spray processing parameters like mesh size, standoff distance, gun travelling speed, and number of passes influence the morphology of the fabricated features; additionally determine the optimal standoff distance between mesh and substrate to fabricate features with optimal deposition efficiency, and determine how the standoff distance between mesh and substrate influences the separation between features and the feature size.

- Investigate how small a two-dimensional surface feature can be fabricated with metal meshes and commercial aluminum powders, the ratio of the pore size of a mesh to the average particle size of feedstock powders for successful cold spray deposition, how geometries of the features can be modified, and what substrate (aluminum, glass, silicon wafer, and printed circuit board) can be patterned using cold-spray surface patterning technique.

- Determine if the cold-spray surface patterning could be a potential technique to create heterogeneous two-dimensional functional features or devices at micron-sized with high efficiency.

THIS PAGE INTENTIONALLY LEFT BLANK

II. EXPERIMENTAL PROCEDURES

A. FEEDSTOCK POWDERS

The feedstock powders considered for this research were 3 μm from Pyro Chem Source, 5 μm from Alpha Chemicals, and -45 to +5 μm (Al 99.5 Min., SST-A5001) from Centerline. Upon simple visual observation, the first two were found to be agglomerated with an appearance of being humid, even after being ultrasonically sieved. Initial coating deposition trials were performed using each powder, which resulted in clogging the system's powder feeder.

Because of this, only the -45 to +5 μm (Al 99.5 Min., SST-A5001) aluminum powder was considered for further characterization techniques. The main characteristics of composition, phase content, and mechanical properties will determine suitability for coating deposition and patterning on the substrates.

B. POWDER AND COATINGS CHARACTERIZATION

1. Particle Size Analysis

The size distribution of the SST-A5001 commercial powder was measured utilizing the HORIBA Laser Scattering Particle Size Analyzer (LA-950V2), which has two wavelength light sources: a 650 nm red laser and 405 nm blue LED. Using a refractive index of 1.6-5.4i, a sample of approximately 100 mg was dispersed in isopropanol and inserted into the analytical Fraction cell.

As a second method for obtaining the powder's average particle size, ImageJ software was used to analyze BSD images (taken with the SEM) of the powder particles. Approximately five measurements were made on more than 100 particles. For accuracy, the results obtained from the software were then compared with those from the LA-950V2.

2. Preparation of Al Powder and Coating Samples

For metallographic analysis, the aluminum powder was mixed with Struers Epofix, stirred continuously for 5 minutes to ensure complete mixing, and then

poured slowly into a plastic mold. For cross-section analysis, the cold-spray deposited coatings on substrates were cold mounted as well. The molds were then left for a 24-hour period to allow them to cure at room temperature to complete the hardening process.

The subsequent preparation consisted of grinding the samples with silicon carbide paper ranging from 320 grit to 2400 grit. Then the samples were manually polished with 1 μm, and 0.25 μm liquid diamond suspension, and then with 0.05 μm colloidal silica polishing suspension using Buehler microcloths. For analysis in the Scanning electron microscope, the samples were coated with 5 nm of palladium, using a Cressington 208HR sputter coater.

3. Scanning Electron Microscopy for Powder and Coatings

With a nominal electron probe current of approximately 1320 pA, secondary electron (SE), with objective aperture of 30 μm, in-lens secondary electron (ILSE), and backscatter detector (BSD) with objective aperture of 60 μm images of the powder microstructure, and sample coatings were captured utilizing a Zeiss Neon 40 FIB-SEM at 20 keV at various magnifications (250X to 20kX).

4. X-ray Diffraction

To determine volume fraction and lattice parameters, X-ray diffraction (XRD) was conducted on the powder. Analysis was performed at room temperature, using a Rigaku Miniflex 600 diffractometer, with a Cu K radiation source, a D/teX Ultra 1D detector, and a 600-watt X-ray generator at 40 kV and 15 mA.

For analysis diffraction, data was collected using a two-scan axis with a step width of 0.02° and a scan speed of 3 degrees/minute across a 2-theta 30–140° scan range. The crystallite size and lattice strain parameters were determined through the Williamson-Hall method using the PDXL software that utilized ICDD database card 03–065-2869.

C. COATING PRODUCTION

The set of experiments were conducted to determine the suitability of the different substrates to be sprayed and get powder attachment to their surfaces, and to examine how small the feature can be created using different masks sizes with this cold-spray surface patterning technique.

For experiments, a Centerline SST model series C low pressure (<300psi) cold gas dynamic spray system (Figure 8), was utilized for the deposition. The system consists of a pressurized spray cabinet, control unit, and an air filtration unit. The parameters for nozzle spray pressure, temperature, feeder vibrational hopper, and feed rate were set in the control unit.

The nozzle selected for spraying the feedstock powder was the De Laval Ultiflow, which is manufactured with a polymer material that is ideally suited to spraying pure Aluminum, Zinc, and Tin without clogging. The dimensions of the nozzle were measured from a cross-section of the nozzle used in the experiment and listed in Table 1. A divergence angle of 6.94° was measured from the nozzle.

Substrates used were aluminum (Series 1100), silicon wafer (Montco Silicon Tech.), silicate glass (Ted Pella Inc.), and PCB (Uxcell). All substrates were cleaned with acetone before use; no substrate treatment, such as anodization or grit blasting, was applied. The carrier gas, pure nitrogen, was routed through the control unit and regulated to spray conditions. The nozzle inlet pressure was 200 psi, with nozzle inlet temperatures ranging from 150 to 300 °C.

Figure 8. Centerline SST Model Series C low-pressure cold spray system installed at the Naval Postgraduate School.

Table 1. Dimensions of de Laval nozzle used in experiments.

Nozzle Parameters	Values, mm.
D_i	4.5
D_t	2.8
D_e	5.6
L_a	14.5
L_b	6.5
L_c	11.5
L_d	87.5

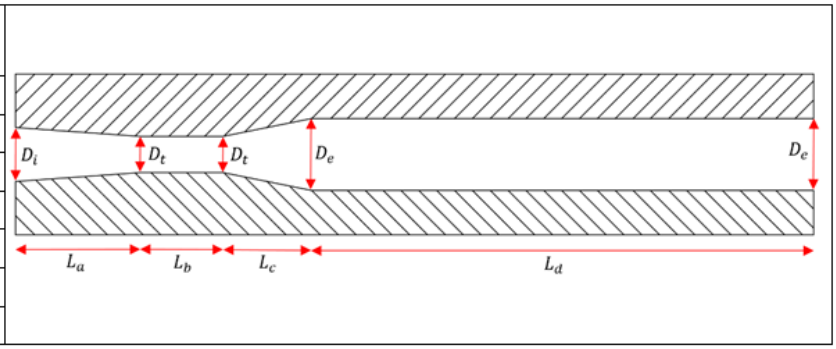

Note: The dimensions were measured from and actual cross-section of the nozzle used. The drawing is not to scale.

1. Masked Cold Spray Deposition Experiments

This experiment focused on fabrication of two-dimensional surface patterns, using different mask sizes, it explored the effect of the feedstock powder's particle size, screen size, standoff distance, gun temperature, gun pressure, gun traverse speed, and substrates on the geometries of the surface patterns, and examined how small a feature was possible with this technique. To produce two-dimensional surface features, five meshes, 16, 45, 170, 200 and 400, were used as screens to block the sprayed particles from deposition. A 3D printed 8 mm ABS plastic mesh was considered as a screen to examine the feasibility of using plastic screen for cold spray surface patterning; however, the plastic mesh deformed transiently with impacting particles with gas temperature of 300 °C (Figure 9), which results in no features patterned on a substrate. To prevent deformation of the plastic mesh, the gas temperature can certainly be reduced below 300 °C, but this will result in no adhesion of aluminum particles to the substrates; therefore, using plastic screen for cold spray surface pattering is determined to be not feasible in our investigation.

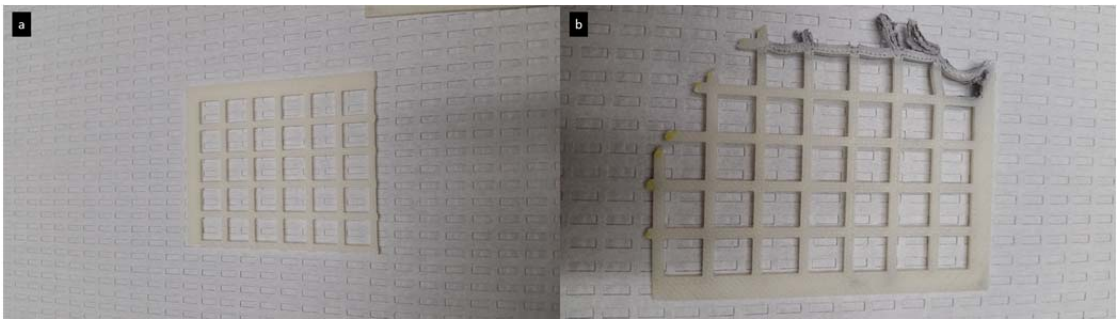

Figure 9. 3D printed ABS mesh (a) as received, and (b) deformed.

The meshes' SEM images are shown in Figure 10; pore and wire size were measured in the SEM. Data are listed in Table 2.

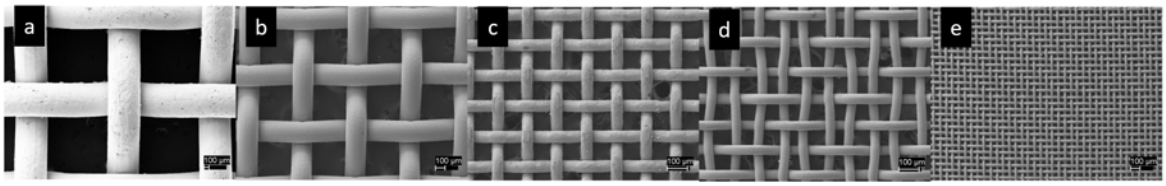

Figure 10. SEM images showing pore and wire size (a) 16, (b) 45, (c) 170, (d) 200, and (e) 400.

Table 2. Pore size and wire size of meshes 60, 45, 170, 200, and 400.

	Mesh 16	**Mesh 45**	**Mesh 170**	**Mesh 200**	**Mesh 400**
Pore Size (µm)	1087.4 ± 9.7	312.8 ± 2.6	87.6 ± 0.9	68.0 ± 5.4	37.3 ± 1.5
Wire Size (µm)	588.9 ± 3.6	197.6 ± 2.6	55.5 ± 0.7	44.8 ± 0.5	25.5 ± 0.2

Standoff distances from the nozzle to the meshes were measured from the bottom of the nozzle to the meshes surfaces; the standoff distances from the meshes to the substrates were measured from the meshes to the substrates' surfaces. The powder then was sprayed onto the substrates utilizing the values listed in Tables 3, 4, and 5.

Table 3. Cold spray parameters utilized on masked PCB substrates.

Substrate	**PCB Sample 4**	**PCB Sample 5**	**PCB Sample 6**	**PCB Sample 7**	**PCB Sample 8**	**PCB Sample 9**	**PCB Sample 10**
Pressure (Psi)	200	200	200	200	200	200	200
Gas Temp. (°C)	245	245	245	245	245	245	245
Feed Rate (g/min)	20	20	20	20	10	20	10
Nozzle Speed (mm/s)	20	20	20	40	20	40	20
Nozzle Step Over per Pass (mm)	1	1	1	1	1	1	1
Mesh Number	16	45	45	45	45	45	45
S.O Distance Nozzle – Mesh (mm)	25	25	25	25	25	25	25
S.O Distance Mesh –Substrate (mm)	1.7	3.7	1.7	1.7	1.7	0	0

Table 4. Cold spray parameters utilized on masked silicon wafer substrates.

Substrate	Glass Sample 1	Si Wafer Sample 1	Si Wafer Sample 2	Si Wafer Sample 3	Si Wafer Sample 4	Si Wafer Sample 6
Pressure (Psi)	200	200	200	200	200	200
Gas Temp. (°C)	320	245	245	245	320	245
Feed Rate (g/min)	40	20	20	20	20	20
Nozzle Speed (mm/s)	20	40	40	40	40	40
Nozzle Step Over per Pass (mm)	1	1	1	1	1	1
Mesh Number	16	16	16	45	5/16″	45
S.O Distance Nozzle – Mesh (mm)	50	25	25	25	50	25
S.O Distance Mesh –Substrate (mm)	3.58	2.37	1	2.37	11	0

Table 5. Cold spray parameters utilized on masked aluminum substrates.

Substrate	Aluminum Sample 1	Aluminum Sample 2	Aluminum Sample 3	Aluminum Sample 4	Aluminum Sample 5	Aluminum Sample 6	Aluminum Sample 7	Aluminum Sample 8
Pressure (Psi)	200	200	200	200	160	200	200	200
Gas Temp. (°C)	320	320	320	300	150	300	300	300
Feed Rate (g/min)	40	40	40	20	15	15	20	20
Nozzle Speed (mm/s)	10	10	20	20	20	20	20	40
Nozzle Step Over per Pass (mm)	1	1	1	1	1	1	1	1
Mesh Number	16	16	16	200	170	400	170	400
S.O Distance Nozzle – Mesh (mm)	25	25	25	15	15	25	25	25
S.O Distance Mesh –Substrate (mm)	2	2	2	0	0	0	0	0

The morphology of the patterned substrates was analyzed with a Dino-Lite digital microscope set for low magnification imaging. Nikon Epiphot 200 metallographic optical microscope and the Zeiss Neon 40 field emission scanning electron microscope set for high magnification imaging were used to measure the feature size of the fabricated features.

The feature heights and three-dimensional topography of the surface patterns were characterized by a Zygo NewView 7100 optical profilometer. All the measurements were conducted in ImageJ. The statistical analyses were carried out in JMP Pro12 software.

THIS PAGE INTENTIONALLY LEFT BLANK

III. RESULTS AND DISCUSSION

A. POWDER CHARACTERISTICS

1. Particle Sizing

The particle sizes of the SST-A5001 powder show a Gaussian distribution (as seen in Figure 11); the range of powder sizes can also be seen. The mean particle size of the powder is shown in Table 6.

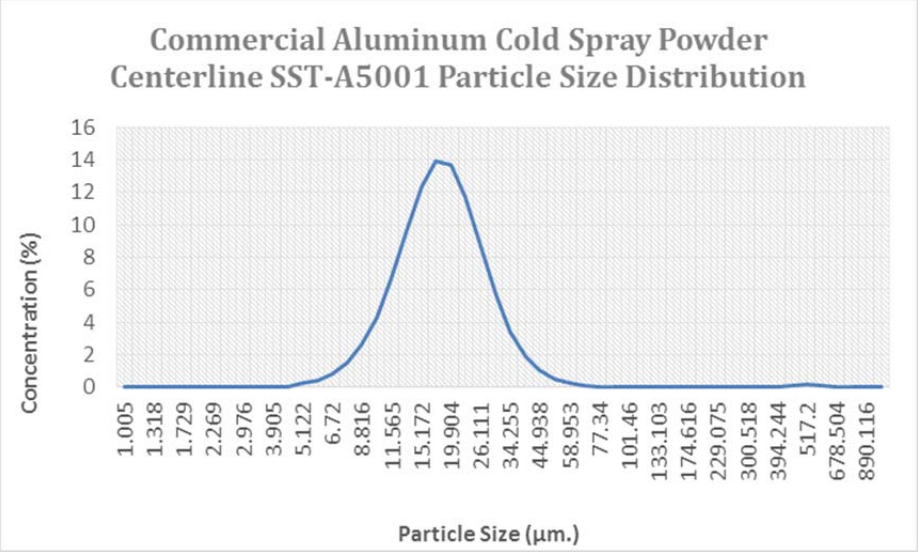

Figure 11. Particle size distribution for the SST-A5001 aluminum powder.

Table 6. SST-A5001 aluminum powder, particle size characteristics.

Powder	Mean Size (µm.)	D10 (µm.)	D90 (µm.)
SST-A5001	20.37179	10.11899	28.33084

2. Particle Morphology

The SEM and ImageJ software were used to analyze the particles' morphology of the SST-A5001 powder. The mean Feret diameter is 12.8 μm, and its 90% confidence interval is within 11.0 and 14.7 μm. These values are within the range of the specifications. The difference shown between the results of the laser scattering analyzer and the SEM might be due to particle geometries. The mean roundness was found to be 0.55, and the aspect ratio 2.07 in the SEM analysis, which indicates that these particles are elongated with an irregular morphology (Figures 12 and 13). One benefit of having these irregular morphologies is that it has been reported that powders with irregular morphologies present a higher velocity than same-size powders with spherical morphologies [42].

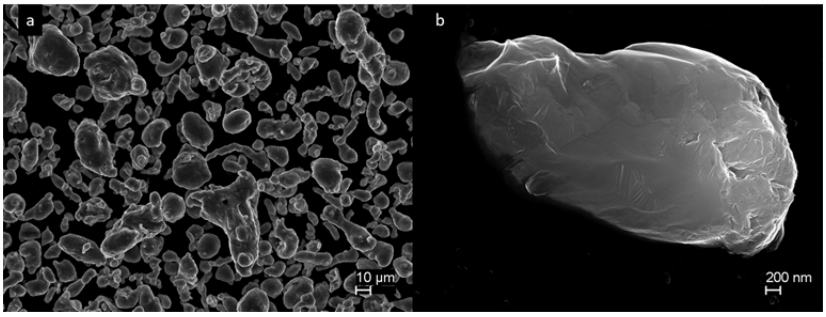

Figure 12. Inlens SEM images of the SST-A5001 aluminum powder (a) 400X, and (b) 20kX Mag.

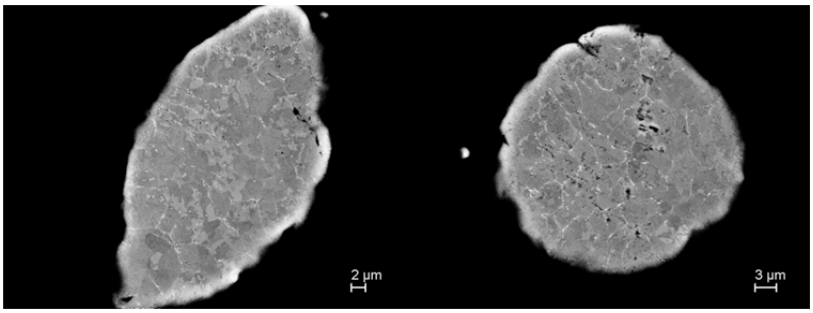

Figure 13. Backscatter detector cross-section images of the SST-A5001 aluminum powder showing their grain structure.

3. X-ray Diffraction

The x-ray diffraction (XRD) data indicates that the SST-A5001 aluminum powder has (FCC) phase; its four strongest diffraction peaks at 2-theta degree values of 38.48, 44.73, 65.10, and 78.23, indicating that the powder is pure aluminum. Phase patterns of the aluminum powder are shown in Figure 14.

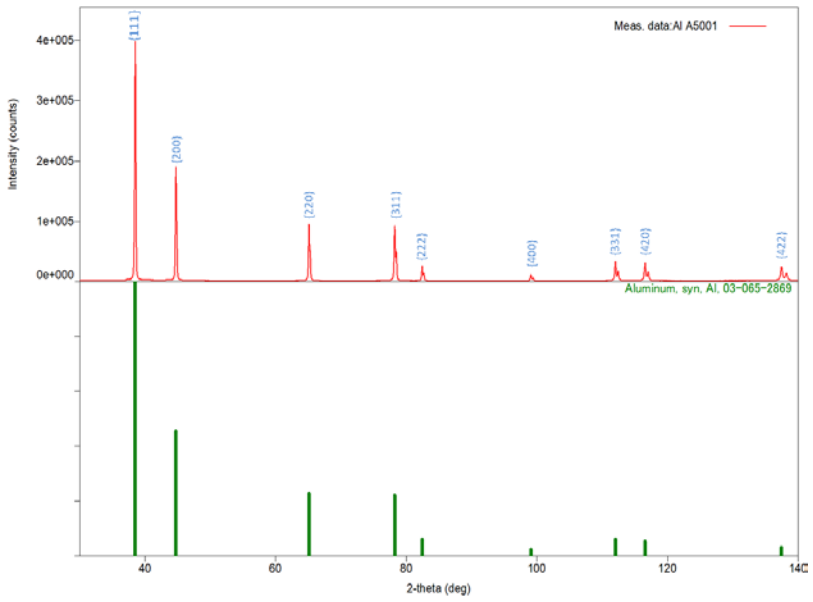

Figure 14. XRD pattern of SST-A5001 Al powder.

B. COLD-SPRAY COATINGS

1. Masks and Substrates

Both copper and stainless steel meshes worked very well for spraying aluminum feedstock powders with gas temperatures above 300°C. All of the copper and stainless steel meshes were found to be reusable for multiple experiments; this reusable nature is cost-friendly for the application of cold-spray surface patterning. Due to its porosity, the adhesion of a cold-sprayed coating to the mesh is poor; even if a coating were formed on top of a fine mesh, it could be removed easily.

Although only metal meshes with square pores were tested in the present study, the findings can certainly be applicable to metal screens with pores in various morphologies. Metal additive manufacturing techniques can potentially be used to fabricate screens with morphologies of interest.

Initially, the nonconductive layer of PCB had been sprayed with aluminum feedstock powders; however, besides the formation of a groove on the substrate caused by erosion from impacting particles, no adhesion of aluminum feedstock powders was obtained (Figure 15). As a result, the copper foil layer was used as a substrate.

Results show that two-dimensional features with various geometries could be fabricated on different substrates including aluminum, silicon, soda-lime glass, and copper foil layer of PCB, as shown in Figure 16. The sample identification (ID), cold spray processing parameters, and the corresponding feature heights are listed in Table 7 for the aluminum substrate, Table 8 for glass and silicon wafer substrates, and Table 9 for PCB substrate, respectively. Detailed discussion on how cold-spray processing parameters influence the fabricated two-dimensional features is described in the following sections.

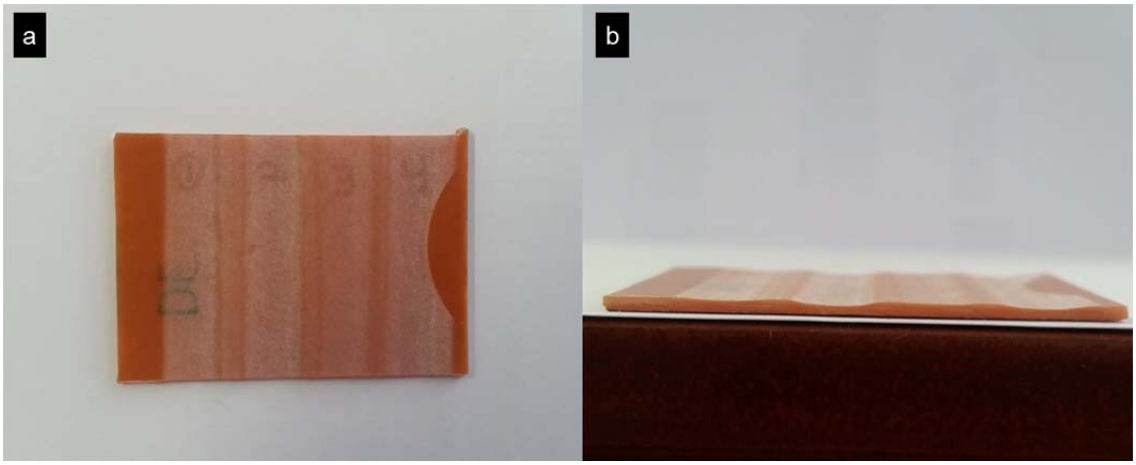

Figure 15. Non-conductive side of PCB (a) surface erosion, and (b) grooves formation.

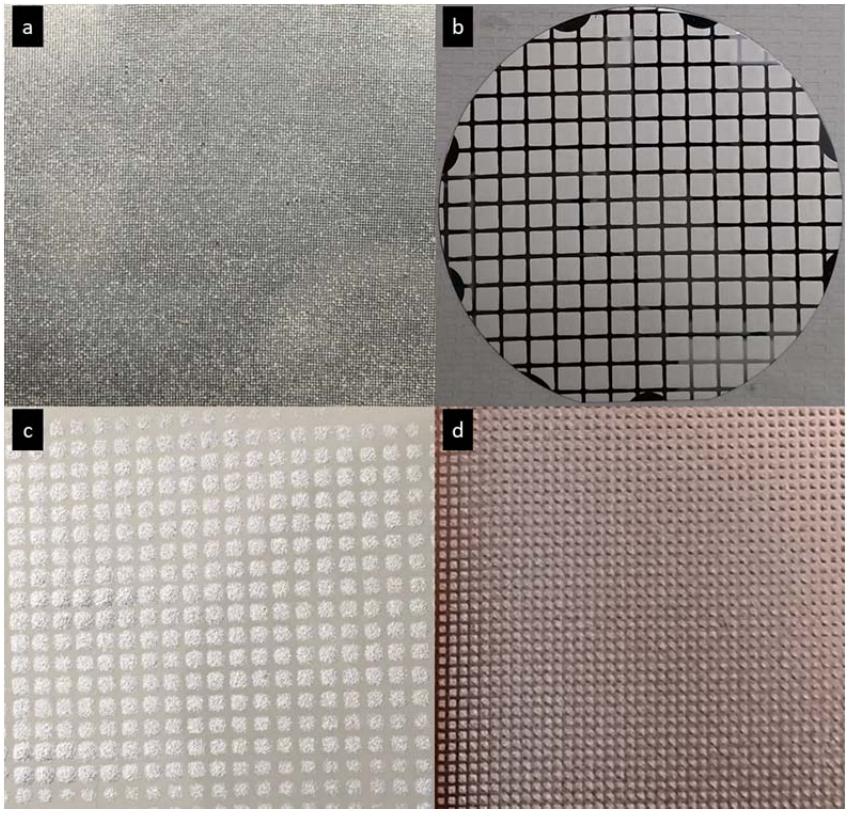

Figure 16. Two-dimensional features fabricated on (a) aluminum, (b) silicon wafer, (c) glass, and (d) copper foil layer of PCB with cold spray surface patterning technique.

Table 7. Cold spray processing parameters and height of features fabricated with meshes (16, 170, 200, and 400), on aluminum substrate.

Parameters	Sample ID							
	Al-1	Al-2	Al-3	Al-4	Al-5	Al-6	Al-7	Al-8
Mesh	16	16*	16	170	170	200	200	400
Pressure (Psi)	200	200*	200	160	200	200	200	200
Gas Temp. (°C)	320	320*	320	150	300	300	300	300
Feed Rate (g/min)	40	40*	40	15	20	15	20	20
Gun Traverse Speed (mm/s)	10	10*	20	20	20	20	40	20
Nozzle Step Over per pass (mm)	1	1	1	1	1	1	1	1
Standoff Distance Nozzle – Mesh (mm)	25	25*	25	15	25	25	25	15
Standoff Distance Mesh – Substrate (mm)	2	2*	2	0	0	0	0	0
Feature Height (µm)	392.3±9.5	760.6±25.6*	59.9±2.1	N/A**	12.0±0.8	8.8±1.2	11.5±2.2	N/A**

*The only data set fabricated with two passes. ** No adhesion of powders.

Table 8. Cold spray processing parameters and height of features fabricated with meshes 16, 45, and 5/16” on glass and silicon wafer substrates.

Parameters	Sample ID					
	Glass-1	Si-2	Si-3	Si-4	Si-5	Si-6
Mesh	16*	5/16"	16	16	45	45
Pressure (Psi)	200*	200	200	200	200	200
Gas Temp. (°C)	320*	320	245	245	245	245
Feed Rate (g/min)	40*	20	20	20	20	20
Gun Traverse Speed (mm/s)	20*	40	40	40	40	40
Nozzle Step Over per pass (mm)	1	1	1	1	1	1
Standoff Distance Nozzle – Mesh (mm)	50*	50	25	25	25	25
Standoff Distance Mesh – Substrate (mm)	3.58*	11	1	2.37	0	2.37
Feature Height (µm)	589.1±165.5*	58.57±9.1	157.8±2.1	175.2±5.5	33.4±3.0	156.9±4.7

* The only data set fabricated on glass substrate.

Table 9. Cold spray processing parameters and height of features fabricated with meshes 16 and 45 on copper foil layers of PCB.

Parameters	Sample ID						
	PCB-1	PCB-2	PCB-3	PCB-4	PCB-5	PCB-6	PCB-7
Mesh	16	45	45	45	45	45	45
Pressure (Psi)	200	200	200	200	200	200	200
Gas Temp. (°C)	245	245	245	245	245	245	245
Feed Rate (g/min)	20	10	20	20	20	20	10
Gun Traverse Speed (mm/s)	20	20	20	20	40	40	20
Nozzle Step Over per pass (mm)	1	1	1	1	1	1	1
Standoff Distance Nozzle – Mesh (mm)	25	25	25	25	25	25	25
Standoff Distance Mesh – Substrate (mm)	1.7	1.7	1.7	3.7	0	1.7	0
Feature Height (µm)	346.1±6.0	255.7±5.2	249.4±11.8	214.2±4.6	86.9±2.4	190.5±4.7	142.4±3.1

2. Pore and Feature Size

Part of the objective of this research is to examine how small the two-dimensional features can be fabricated with the cold spray surface patterning technique. Mesh (16, 170, 200 and 400) were used as screens to block the impacting particles from deposition to fabricate two-dimensional surface features on aluminum substrates. During the cold-spray surface patterning process, the screens were secured above the substrates with a standoff distance of 2 mm for features fabricated with mesh 16 (samples Al-1, Al-2, and Al-3), and a standoff distance of 0 mm for features fabricated with mesh 170, mesh 200, and mesh 400 (samples Al-4, Al-5, Al-6, Al-7, and Al-8). The pore and wire sizes of the

meshes, feature sizes, and feature heights were measured in the SEM and optical profilometer. The sample IDs and the representative average data (with margin of errors) are listed in Table 10, and the corresponding cold-spray processing parameters are listed in Table 7. Surface features were created with mesh 16, mesh 170, and mesh 200 successfully, but not with the mesh 400, which has pore size of 37.3 ± 1.5 μm and wire size of 25.5 ± 0.2 μm. This result is understandable because reduction of pore size also reduces the probability of impacting particles passing through the mesh. Once the pore size of a mesh is reduced to a critical size or below, the impacting particles can no longer pass the mesh.

Table 10. Sample IDs, pore and wire size of meshes (60, 170, and 400), feature size and height of the patterns fabricated on aluminum substrate.

Measurements	**Sample ID**		
	Al-1	**Al-5**	**Al-7**
Mesh	16	170	200
Pore Size (μm)	1087.4 ± 9.7	87.6 ± 0.9	68.0 ± 5.4
Wire Size (μm)	588.9 ± 3.6	55.5 ± 0.7	44.8 ± 0.5
Feature Size (μm)	1282.5 ± 27.7	100.4 ± 4.3	67.4 ± 3.1
Feature Height (μm)	392.3 ± 9.5	12.0 ± 0.8	11.5 ± 2.2

Figures 17 (a), (b), and (c) show the SEM images of mesh 16, mesh 170, and mesh 200, respectively, as shown in the images, the metal wires in mesh 16 and mesh 170 are well-aligned to each other; however, those in mesh 200 appear wavy. These observations are in accordance with expectations based on pore size. The margin of error of pore size in mesh 200 is relatively high compared to the average pore size. This high margin of error was found to influence the margin of error of the feature size accordingly.

The features fabricated with mesh 16, mesh 170, and mesh 200, are shown in Figures 17 (d), (e), and (f). Well-defined two-dimensional arrays of features were fabricated, especially the features fabricated with mesh 16, which

have distinct square features replicating the square pores of the mesh. Although both features fabricated with mesh 170 and mesh 200 are in well-aligned arrays, each individual feature has irregular morphology. Due to feedstock powder size being relatively big (compared to the pore sizes of mesh 170 and mesh 200), and only a small amount of the impacting particles can be deposited on the substrate to form surface features. Thus, each individual feature was only composed of small amount of particles, resulting in irregular morphology.

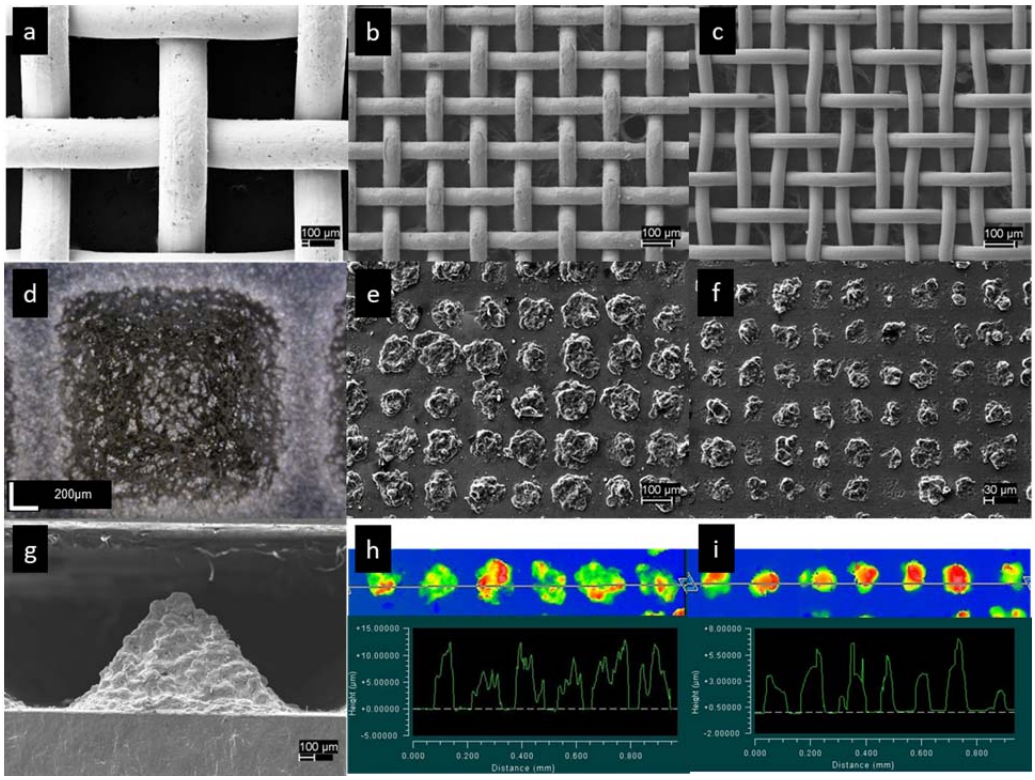

Figure 17. SEM images show the morphology of (a) mesh 16, (b) mesh 170, and (c) mesh 200; the morphology of the features fabricated with (d) mesh 16, (e) mesh 170, and (f) mesh 200; the topography of the feature fabricated with (g) mesh 16. Line profiles of the feature heights of features fabricated with mesh 170 and mesh 200 obtained by optical profilometer are shown in (h) and (i), respectively.

One interesting observation found in the features fabricated with mesh 16 and mesh 170 is that the feature size is actually larger than the pore size. The

basis of this for mesh 16 is that a 2 mm standoff distance between the mesh and substrate was used during the fabrication process. This small spacing allows small amounts of the impacting particles to get beneath the mesh, leading to larger feature size. However, no standoff distance between the mesh and substrate was used for fabrication of features with mesh 170, so the enlargement of the features is not due to the standoff distance, but possibly the screen (metal mesh) being unsecured during the cold-spray surface patterning process. Without proper screen clamping, the patterns cannot be fabricated successfully. Minor movement of a screen might occur during the traverse movement of the gun and result in particles being sprayed underneath the meshes and, therefore enlargement of the feature size. Although both features fabricated with mesh 16 and mesh 170 (samples Al-1 and Al-5) are larger than the pore size, the features fabricated with mesh 200 (sample Al-7) were found to be consistent with average pore size.

As shown in Figure 18, all feature sizes of sample Al-7 are within the expected range; the mean and variance of the feature and pore size are also very similar. A two sample t-test was conducted for feature sizes fabricated with mesh 200 and pore size of mesh 200 (sample Al-7). The p-value of the t-test is 0.84, which is higher than the significance level of 0.05, indicating that the patterned features fabricated with mesh 200 and zero standoff distance replicated the morphology of the pore regions of the mesh 200 very well. The smallest features created in the study were fabricated with mesh 200 and have an average feature size of 67.4 μm, which is approximately 3.3 times of the average particle size measured from laser scattering analysis. It was not possible to fabricate features with the mesh 400, which has an average pore size approximately 1.8 times of the average particle size. Based on the above results, in the present study the pore size needs to be larger than 3.3 times the average particle size of feed stock powders in order to have successful deposition of patterned features.

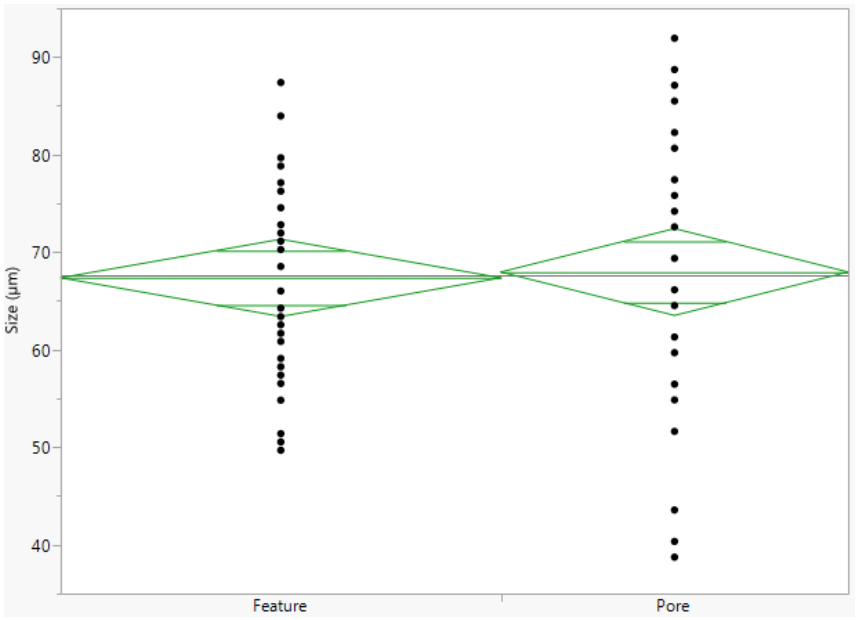

Figure 18. Size distribution of features fabricated with mesh 200 and pore size of mesh 200. The diamond shows the 95% confidence intervals of individual data set and one-way analysis of variance data.

The feature heights of the samples were also examined in the SEM and optical profilometer; the data are shown in Figures 17 (g), (h), and (i). As shown in Figure 17 (g), when the pore size is much bigger than the particle size, the two-dimensional feature tends to form in a pyramid. This observation was also found in the fin arrays produced by Y. Cormier et al. [27], [29], [43]. The formation of this pyramid-shaped morphology was not done intentionally, but likely attributable to the divergent spray of feedstock powders through the de Laval nozzle and the recirculation zone generated near the edges of the meshes. With a nozzle sitting in one location of a substrate for 200 seconds, a cone-shaped feature formed; no further adhesion of the impacting particles was observed with increased spraying time (Figure 19 (a)). The angle between the edge of the cone and the horizontal substrate was measured to be approximately 77°. This demonstrates that, even without a screen, a cold-sprayed coating was formed with inclined edges. In addition to the divergent angle introduced by the gun, the recirculation zone played an important role for

the formation of the pyramid-shaped morphology [13], [44]. A schematic drawing of how a recirculation zone appeared near the edges of a screen is shown in Figure 19 (b).

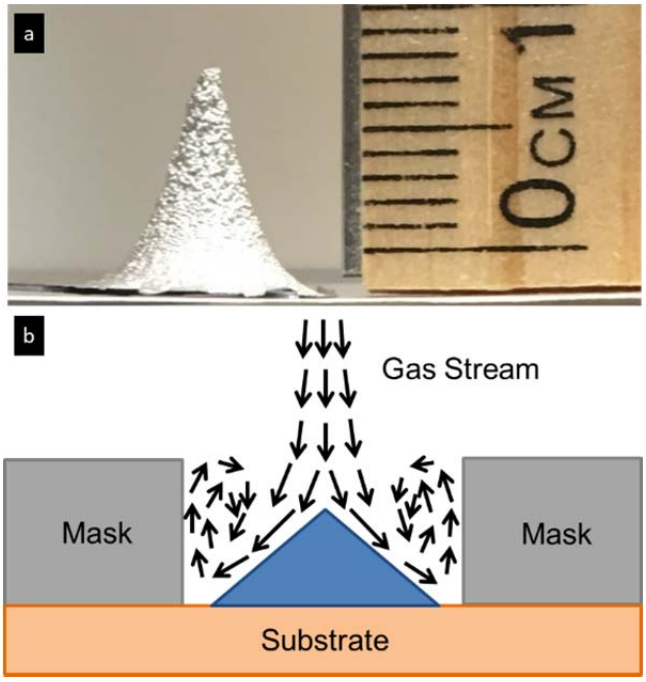

Figure 19. (a) Optical image of cold sprayed coating at a single location with duration of 200 seconds. (b) Schematic drawing of the recirculation zone near the edges of a screen (not to scale).

The average feature heights fabricated with mesh 170 and mesh 200 were found to be very similar (samples Al-5 and Al-7). The two-sample t-test gave a p-value of 0.60, which indicates that both feature heights are statistically indistinguishable. The 40 mm/s gun traverse speed, used for the fabrication of features with mesh 200 (sample Al-7) was 2 times higher than the parameter used for the fabrication of features with mesh 170 (sample Al-5). Thus, the duration of the cold spray for mesh 170 should be 2 times higher than the time sprayed with mesh 200. However, this longer duration of the spray was not reflected in the feature heights. One main reason for this is that after one pass of cold spray, both of the tops of the mesh 170 and mesh 200 were fully covered

with a layer of cold sprayed coating. This prevented further deposition of any particles; therefore, adjustment of the feature height for mesh smaller than 170 can be challenging. Finer powders with non-agglomerated property might be a potential solution for this problem.

It is worth noting here that changing the screen used for the patterning not only affects the feature size, but also the feature height. Two pairs of samples (Si-4 and Si-6; PCB-1 and PCB-2), which share identical cold spray processing parameters but different mesh size, have different feature heights, as shown in Table 8 and Table 9. The samples (Si-4 and PCB-1) fabricated with mesh 16 have feature heights of 175.2 ± 5.5 μm and 346.1 ± 6.0 μm, respectively. In contrast, the samples (Si-6 and PCB-3) fabricated with mesh 45 have feature heights of 156.9 ± 4.7 μm and 249.4 ± 11.8 μm. This result shows that the feature height tends to be higher when using bigger meshes (lower mesh numbers). The source of this result is likely due to the formation of a recirculation zone generated near the edges of a mesh. Mesh with smaller pores may lead to a higher backflow of gas stream near a substrate, which reduces the momentum of impacting particles and prevents particles bonding.

The SEM images in Figures 20 (a) and (b) show the aluminum cold-sprayed features fabricated with mesh 16 and mesh 45 on a copper foil layer of PCB; Figures 21 (a) and (b) show the aluminum features fabricated with mesh 16 and mesh 45 on a silicon wafer substrate. Both features fabricated with mesh 16 are higher than the ones fabricated with mesh 45. Again, the pyramid-shaped morphologies were found in all the features, despite the substrates used being PCB and silicon wafer rather than aluminum.

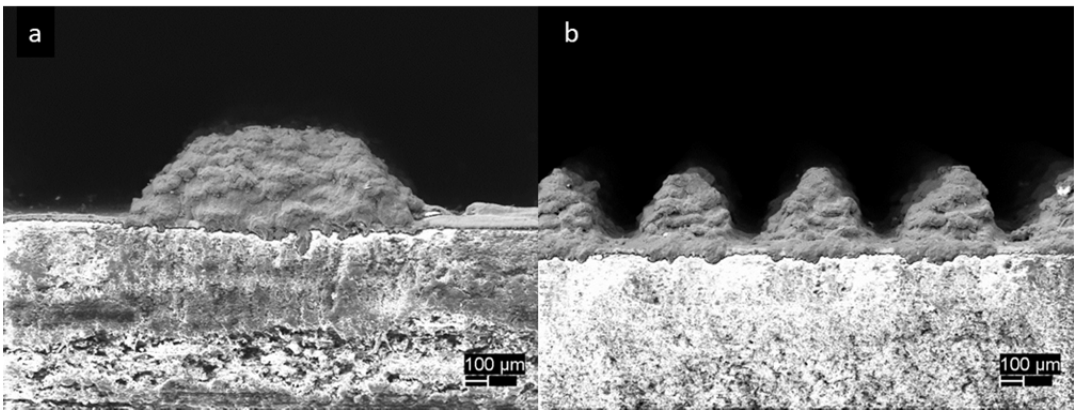

Figure 20. SEM images of aluminum cold sprayed features fabricated with (a) mesh 16 and (b) mesh 45 on a copper foil layer of PCB.

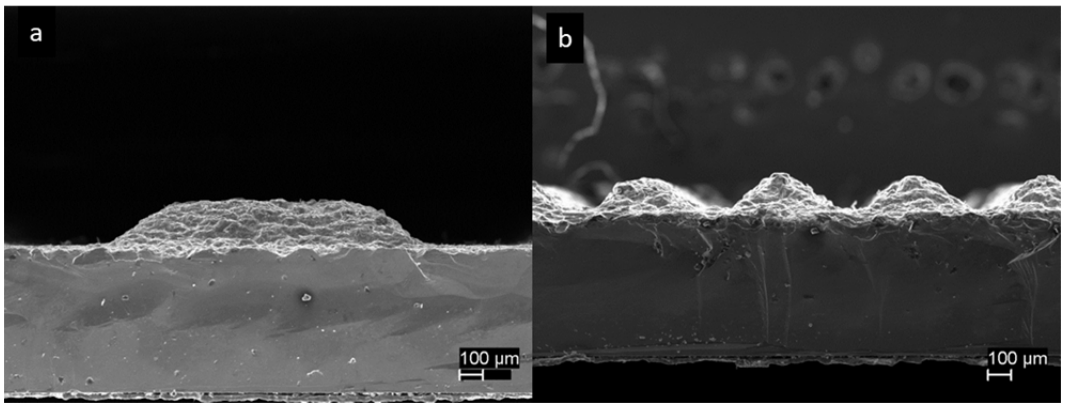

Figure 21. SEM images of aluminum cold sprayed features fabricated with (a) mesh 16 and (b) mesh 45 on silicon wafer substrate.

3. Monte Carlo Simulation

In cold-spray surface patterning, the basic principle of using a screen to mask regions where exposure to impacting particles is undesirable is similar to that used in lithography. However, the impacting particles in cold spray are not identical to the photons used in lithography; they have significantly larger mass and volume, which limit their ability to pass through a metal mesh. In the present study, a Monte Carlo simulation was developed to estimate the probability of feedstock powders passing through the meshes and depositing on the substrates. The simulation only uses the particle size distribution measured from laser-scattering analysis, with the average wire width and pore size listed in

Table 10 as input parameters. The morphologies of particles used in the simulation were all spherical. In each simulation 1000 Monte Carlo steps were simulated for mesh 16, mesh 170, mesh 200, and mesh 400; ten simulations were run for each sample. The average probabilities of particles passing the mesh 16, mesh 170, mesh 200, and mesh 400, are 40.4%, 21.9%, 18.2%, and 8.3%, respectively. The above probabilities only consider the geometry of the particles and meshes; they do not take into account the effect of particle size to the critical velocity. Several reports suggested that the particle size might influence the critical velocity for cold-spray deposition [30], [45]. Possible reasons include higher amounts of contaminants or oxides on the surfaces of smaller particles, (which have high surface-to-volume ratio), preventing the bonding formation, or the higher cooling rate of smaller particles possibly hindering the occurrence of shear instabilities [30], [46]. All these factors result in an increase of critical velocity for fine particles. T. Schmidt et al. stated an equation to estimate a "critical particle diameter" (d_{crit}) for cold spray deposition [30]. Particles with diameters above the critical particle diameter have slow thermal diffusion which allows localized shear instability to occur at the surface of impacting spherical particles. The equation is listed as follows [30]:

$$d_{crit} = 36 \times \frac{k}{c_p \, \rho \, v_{particle}}$$

where k is the thermal conductivity, c_p is the specific heat, ρ is the density, and $v_{particle}$ is the particle velocity. The particle velocity used in the present study was not measured in the experiment; however, J. F. Schiel has created a one-dimensional model of the fluid dynamics and particle transport properties to estimate particle velocity of cold sprayed particles for the Centerline SST model series C Ultilife nozzle. The simulated particle velocities have been compared and show good consistency with the data measured with a laser velocimetry. This model was utilized to estimate the particle velocity with our cold spray processing parameters: aluminum feedstock powders, 1.37 Mpa (200 psi), 300 °C, and transport gas of nitrogen. The particle velocity was estimated to be

558 m/s. With the inputs of particle velocity, thermal conductivity, specific heat and density of aluminum, the critical particle diameter was estimated to be 5.1 μm, which is below 0.26 percentile of the total particle size distribution measured from laser scattering analysis. Thus, no obvious change was found in the result of Monte Carlo simulation incorporating the critical particle diameter. However, if the deceleration of the smaller particles (due to bow-shock near the substrate) is also taken into account; the optimum size range for most materials falls within -45 to 10 μm [30], [39].

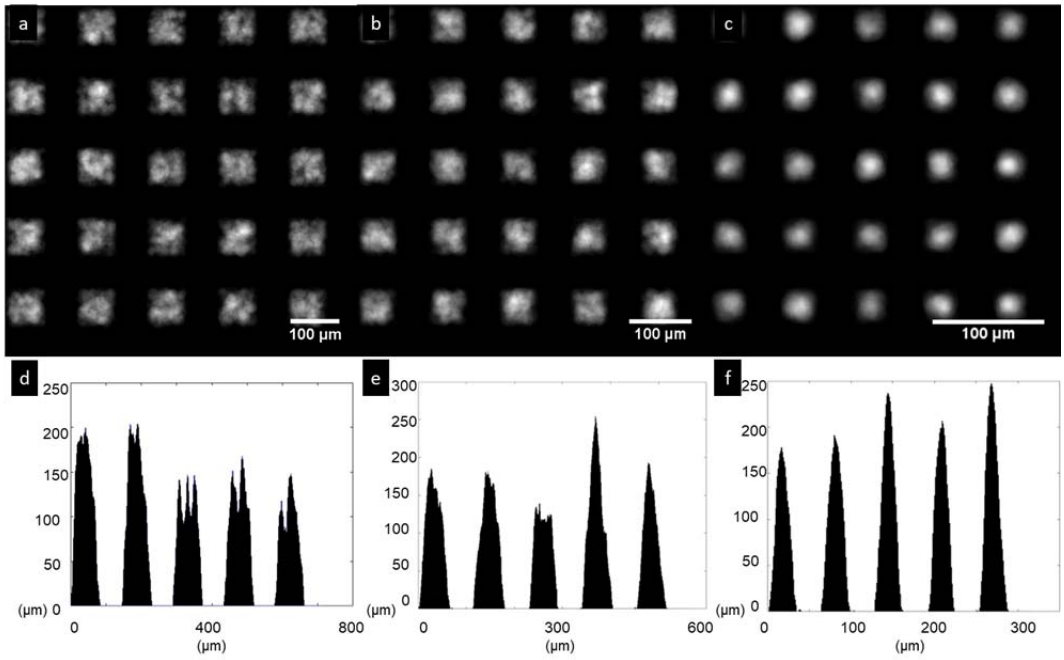

Figure 22. Simulated features of (a) mesh 170, (b) mesh 200, and (c) mesh 400 by Monte Carlo simulation with 25,000 particles and experimental particle size distribution measured by laser scattering analysis. Successful bonding of particles to the substrates was limited to feedstock powders with particle size of 10 μm and above. The corresponding line profiles of the vertical center features in (a), (b), and (c) are shown in (d), (e), and (f).

If the deposition of the particles in the Monte Carlo simulation is limited to particle sizes larger than 10 μm, the deposition probabilities further decrease to 37.8%, 20.6% 16.3%, and 6.7% for mesh 16, mesh 170, mesh 200, and mesh

400, respectively. The corresponding simulated cold sprayed features fabricated with mesh 170, mesh 200, and mesh 400, are shown in Figures 22 (a), (b), and (c). The topography shown in Figures 22 (a) and (b) were found to be similar to the experimental data shown in Figures 17 (e), (f), (h), and (i). The line profiles of the vertical center simulated features in Figure 22 (a), (b), and (c) are shown in Figures 22 (d), (e), and (f). The line profiles of the simulated features fabricated with mesh 170 and mesh 200, which are shown in Figures 22 (d) and (e), were also found to be similar to the line profiles of experimental features obtained by an optical profilometer in Figures 17 (h) and (i). The main difference was height; the experimental features are much lower than the simulated data. The primary reasons for this are: as we did not know the actual number of impacting particles sprayed in the experiments, an arbitrary number of particles (25000) was chosen in the simulations; deposition efficiency was not considered in the simulations; and the fine meshes (higher than 170) were usually covered with a coating after one pass of a cold spray. No more particles can pass a coated mesh, so the features can only be formed with the particles passing the mesh initially, which lead to a limited feature height. It is worth noting that, as the probability for bigger particles to deposit at the center of the pores is higher than that of the smaller particles, the center of the simulated features was higher than the areas near the edges of the meshes.

In the simulation, the probability for particles to deposit with mesh 400 is 6.7%, but in actual experimental data there were no features found in samples fabricated with mesh 400. It is possible that the simulation did not take the incident angle of the impacting particles into account. With part of the impacting particles being tilted relative to the normal of a substrate, the probability of passing through the pores of the mesh is even lower. Furthermore, the decelerating of sprayed particles due to bow-shock, which can reduce the velocity of smaller impacting particles below critical velocity and result in no adhesion between particles and a substrate, was not considered in the simulation. Some dented marks generated by the impacting particles were

observed on the surface of substrate sprayed with mesh 400, but no adhesion of particles was found. This indicates that the particles did get through the mesh 400 but no adhesion was formed. Although, the actual geometry of the feedstock powders was not considered in the simulation, many feedstock powders have elongated irregular shapes (as shown in Figure 12(a)), which might further prevent the particles passing through the pores. Thus, in reality, the actual deposition probability could be lower than the simulated value of 6.7%.

4. Standoff Distance between Mesh and Substrate

One aspect of the cold spray surface patterning that was important to investigate was the influence on the morphology of fabricated features exerted by the standoff distance between the mesh and the substrate. The standoff distances of 0 mm, 1 mm, 1.7 mm, 2.37 mm, and 3.7 mm were used for fabrication of aluminum features on copper foil layers of PCB substrates and silicon wafer substrates. Five paired data sets were fabricated (samples PCB-5 and PCB-6, samples PCB-7 and PCB-2, samples PCB-3 and PCB-4, samples Si-5 and Si-6, and samples Si-3 and Si-4), and each data set comprised a pair of features fabricated with the same cold-spray processing parameters except for the standoff distances. The details of the cold-spray processing parameters of the data sets are listed in Tables 8 and 9. The feature heights versus the standoff distance between mesh and substrate of the five data sets are plotted in Figure 23. A general trend appears in the plotting, showing that the feature heights increase along standoff distances of 0 mm to ~2.37 mm; however, the feature heights start decreasing with the increase of standoff distances of ~2.37 mm to 3.7 mm.

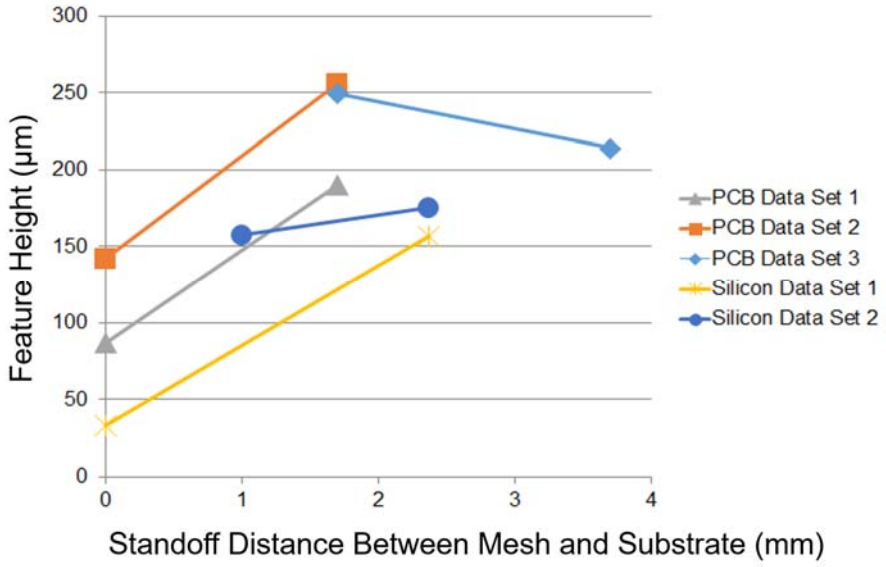

Figure 23. The feature heights versus the standoff distances between meshes and substrates of the five paired data sets fabricated with standoff distances of 0mm, 1mm, 1.7mm, 2.37mm, and 3.7mm on PCB and silicon substrates.

Each data set comprises a pair of features fabricated with the same cold-spray processing parameters except for the standoff distances. The data appears to support an optimal standoff distance for cold-spray surface patterning for fabricating features with optimal deposition efficiency [27], [39]. This possibly is because when the mesh is very close to the substrate the bow-shock and the recirculation of gas flow generated near the substrate is more intense, thus reducing the velocity of the impacting particles and lowering the deposition efficiency [13], [39]. Furthermore, if the standoff distance is too far from the substrate, the particle velocity can be higher than the gas velocity, which leads to a negative drag force on the particles and reduces the deposition efficiency [39]. In the experiments, a 25 mm standoff distance between gun and mesh, and a 2.37 mm standoff distance between mesh and substrate were the optimal conditions for cold-spray surface patterning.

Besides the change of feature height with the standoff distance, it was found that a higher standoff distance between mesh and substrate leads to more

particles sprayed beneath the mesh and a smaller separation between the features.

The optical and SEM images in Figure 24 show the morphology of the patterned features presented the five data sets mentioned above. The samples fabricated with 0 mm and 1.7 mm standoff distances (PCB-5 and PCB-6) are shown in Figures 24 (a) and (b); the samples fabricated with 0 mm and 1.7 mm standoff distances (PCB-7 and PCB-2) are shown in Figures 24 (c) and (d); the samples fabricated with 1.7 mm and 3.7 mm standoff distances (PCB-3 and PCB-4) are shown in Figures 24 (e) and (f). Reduction in the separation between features correlated with the increase of the standoff distances as observed in Figures 24 (a) through (f). Additionally, the samples fabricated with 0 mm and 2.37 mm standoff distances (Si-5 and Si-6) are shown in Figures 25 (a) and (b); the samples fabricated with 1 mm and 2.37 mm standoff distances (Si-3 and Si-4) are shown in Figures 25 (c) and (d).

The same trend was observed in the features fabricated on the silicon wafer substrate. Observations indicate that with smaller standoff distances between mesh and substrate, the separation between the features becomes more pronounced. Although both feature height and the separation between features are affected by the standoff distances, the morphologies of the features above are all pyramid-shaped, despite the materials of substrates used in the cold spray.

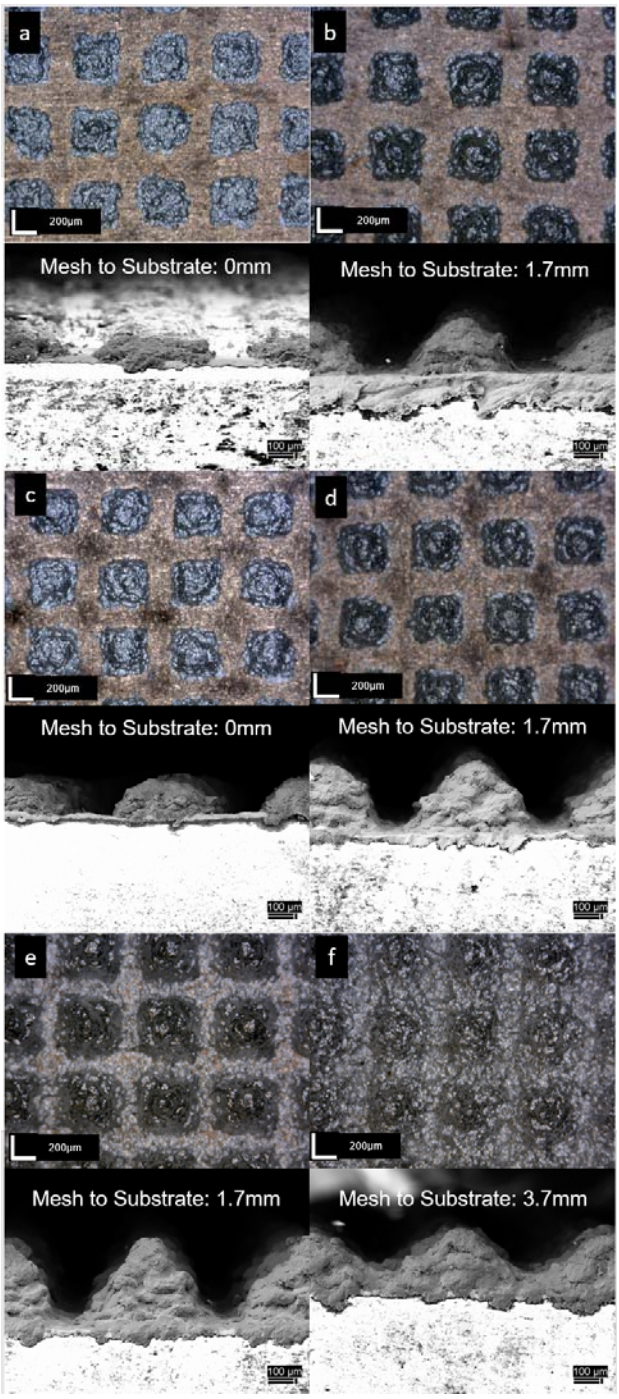

Figure 24. The samples PCB-5 and PCB-6, fabricated with 0 mm and 1.7 mm standoff distances, are shown in (a) and (b); the samples PCB-7 and PCB-2, fabricated with 0 mm and 1.7 mm standoff distances, are shown in (c) and (d); the samples PCB-3 and PCB-4, fabricated with 1.7 mm and 3.7 mm standoff distances, are shown in (e) and (f). Note: the samples listed here represent the data shown in Figure 23.

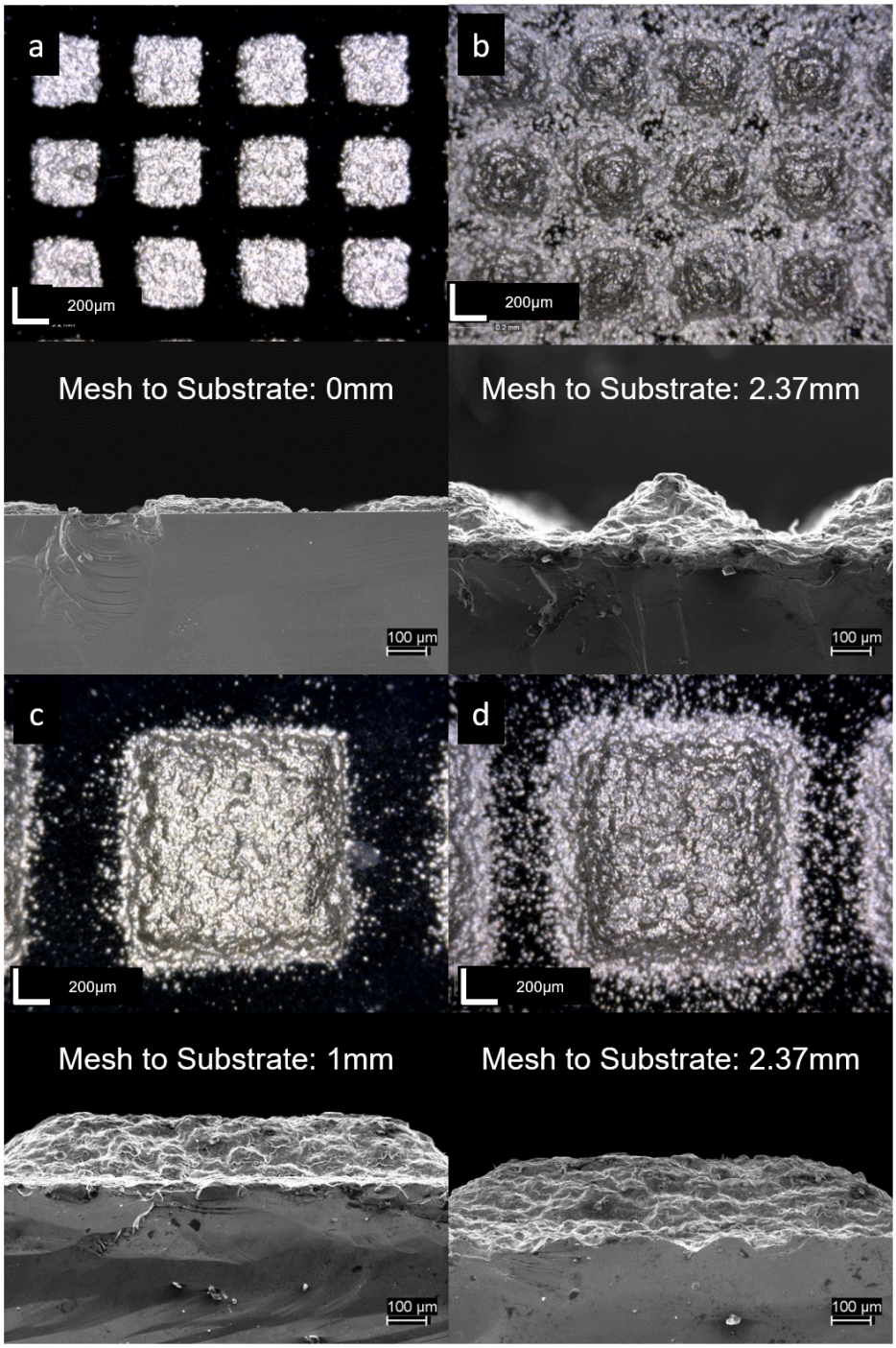

Figure 25. The samples Si-5 and Si-6, fabricated with 0 mm and 2.37 mm standoff distances, are shown in (a) and (b); the samples Si-3 and Si-4, fabricated with 1 mm and 2.37 mm standoff distances, are shown in 25 (c) and (d). Note: the samples listed here represent the data shown in Figure 23.

5. Gun Traverse Speed and Number of Passes

In normal cold spray coating, if the sprayed particles exceed the critical velocity, the coating thickness can be controlled simply by changing the gun's traverse speed and number of passes. The total mass deposit is a simple calculation: feed rate times the distance of travel divided by the gun's traverse speed. With a slow gun traverse speed, or additional passes, more materials can be deposited on a substrate. To examine whether these parameters also influence the feature height, aluminum powders were sprayed with mesh 16 on aluminum substrates with the same cold-spray processing parameters except for the traverse speeds. The same type of experiment was also conducted with mesh 45 on copper foil layers of PCB. The cold-spray processing parameters and the feature heights are shown in Table 9. Despite the different substrates and meshes used, a general trend was found: When the gun's traverse speed is increased, the dwell time of the nozzle on top of the screens is reduced. In features fabricated with mesh 16, the average feature height dropped from 392.3 to 59.9 μm with an increase of gun traverse speeds of 10 to 20 mm/s; and this held true with the features fabricated with mesh 45 as well. The average feature height dropped from 249.4 to 190.5 μm with an increase of gun traverse speeds of 20 to 40 mm/s. Thus, the feature height can be reduced by increasing the gun traverse speed.

The morphology of the features was examined in both optical microscope and SEM. Features fabricated with mesh 16 and gun traverse speeds of 10 and 20 mm/s are shown in Figures 26 (a) and (b). The features fabricated with mesh 45 and gun traverse speeds of 20 and 40 mm/s are shown in Figures 26 (c) and (d). Again, the pyramid-shaped morphologies were found in the features. Modifications in cold-spray processing parameters produced no changes in the pyramid-shaped morphology.

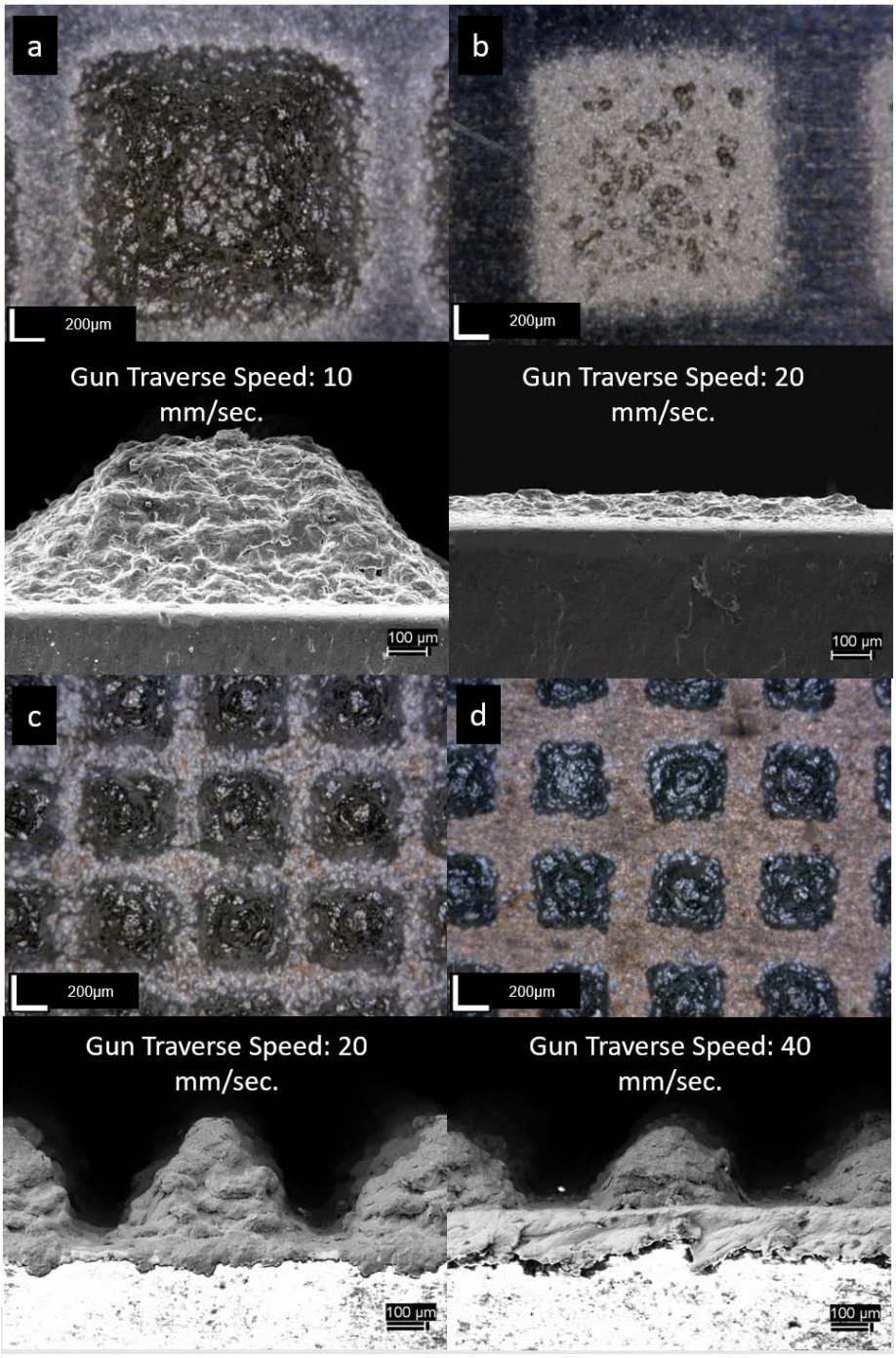

Figure 26. Optical Images and SEM images of aluminum features fabricated with mesh 16 and gun traverse speeds of (a) 10 mm/s, and (b) 20 mm/s, with mesh 45 and gun traverse speed of (c) 20 mm/s, and (d) 40 mm/s.

The influence of the number of passes was examined by spraying one and two passes of aluminum powders with mesh 16 on aluminum substrates with the same cold-spray processing parameters (samples Al-1 and Al-2), as shown in Table 7.

The feature fabricated with one pass is shown in Figure 27 (a), and the one with two passes is shown in Figure 27 (b).The height of the two dimensional features fabricated with one pass was 392.3 ± 9.5 μm; the height of the features fabricated with two passes was 760.6 ± 9.5 μm. Although the features fabricated with two passes were higher, the feature height was not proportional to the number of passes. The morphologies of the features were examined with the SEM. The morphologies of both features stayed as pyramids, but the angles between the edges of the features and the substrates increased from 40° to 52° with spray increase of one pass to two passes. As having the morphology of a pyramid (flat pyramid), the top flat area reduces with the increase of the feature height, which means that less flat area is available for cold-spray deposition. Once a feature reaches a critical height, no further deposition can occur and, the feature will ultimately form a pyramid with sharp tip on top. As shown in Figure 27 (b), there is no flat area remaining on top of the pyramid-shaped feature; because of this geometry, the impacting particle will simply bounce off the feature rather than adhere to it. A similar result was also found in one-dimensional features fabricated by Kim et al. They reported that the aspect ratio (feature height divided by feature width) of the copper electrodes deposited by cold spray increases with number of passes [13]. With seven passes, a film formed at the tip of prism-shaped copper electrode [13]. The formation of pyramid-shaped geometry in the two-dimensional features limited the addition of feature heights. This explains why the average feature heights fabricated with two passes is not equal to twice the average feature heights fabricated with one pass. This limitation of feature heights, due to the pyramid-shaped morphology, might limit

the application of cold-spray surface patterning. Tilting of the nozzle or the substrate might resolve the issue, but further investigation is needed to address this problem.

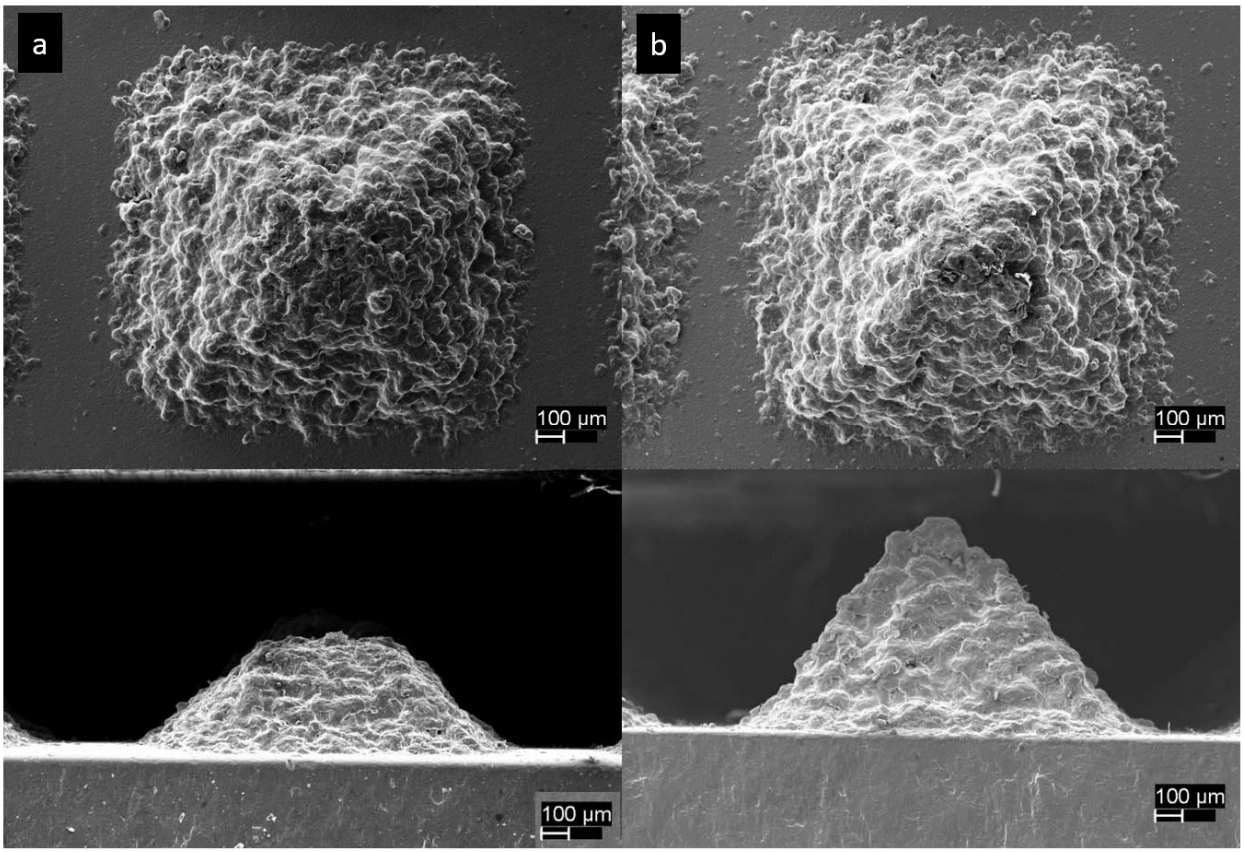

Figure 27. SEM images of aluminum features fabricated with (a) one pass and (b) two passes.

THIS PAGE INTENTIONALLY LEFT BLANK

IV. CONCLUSION

The current study presents the feasibility of fabricating two-dimensional features with aluminum feedstock powders on aluminum, silicon, soda-lime glass, and copper foil layers of PCB substrates. It was found that the two-dimensional features could be fabricated with copper and stainless steel screens on the substrates listed above. More precisely, features could be fabricated with mesh 16, mesh 45, mesh 170, and mesh 200, but not mesh 400. The smallest features that could be fabricated with 45 to +5 μm feedstock powders had an average feature size of 67.4 ± 3.1 μm. The smallest mesh pore size needs to be approximately 3.3 times larger than the average feedstock powders particle size in order to have successful deposition. The feature height was found to be influenced by the mesh number, the standoff distance between mesh and substrate, the gun's traverse speed, and the number of passes. Generally speaking, smaller mesh numbers, slower gun traverse speeds, and higher numbers of passes result in higher feature heights. There is an optimal standoff distance between mesh and substrate for fabricating features with optimal deposition efficiency. Additionally, the standoff distance between the mesh and substrate influences the separation between features and the feature size. With a high standoff distance, overlapping occurs and the feature size increases. To have optimal separation between features and an optimal replication of the morphology of a mesh, zero standoff distance between mesh and substrate should be used. All the features fabricated in the investigation displayed pyramid-shaped morphology. The maximum feature height is limited by the pyramid-shaped morphology. For fabrication with mesh 170 or higher, the feature height was further limited by cold sprayed coating formed on the fine mesh.

The Monte Carlo simulation, incorporating the measured particle size distribution and the geometries of the metal screens, demonstrated to be a useful tool for estimating the probability of feedstock powders passing through the meshes. Both the morphologies and the line profiles of simulated features

fabricated with mesh 170 and mesh 200 showed good correlation with the experimental data, indicating that the Monte Carlo simulation is also a valuable tool for the simulation of surface morphology and topography of features fabricated by the cold-spray surface patterning technique.

LIST OF REFERENCES

[1] Y. Zabila, M. Perzanowski, A. Dobrowolska, M. Kąc, A. Polit, and M. Marszałek, “Direct laser interference patterning: Theory and application,” in *Acta Physica Polonica A*, 2009, vol. 115, no. 2, pp. 591–593.

[2] K. Schuegraf and K. Seshan, “Handbook of thin film deposition processes and techniques: Principles, methods, equipment and applications,” *Angew. Chemie*, vol. 101, p. 646, 2002.

[3] M. Henini, “Handbook of thin-film deposition processes and techniques,” *Microelectronics J.*, vol. 31, no. 3, p. 219, 2000.

[4] D. L. Smith and D. W. Hoffman, “Thin-film deposition: Principles and practice,” *Phys. Today*, vol. 49, no. 4, p. 60, 1996.

[5] M. M. Ling and Z. Bao, “Thin film deposition, patterning, and printing in organic thin film transistors,” *Chemistry of materials*, vol. 16, no. 23. pp. 4824–4840, 2004.

[6] L. R. Harriott, “Limits of lithography,” *Proc. IEEE*, vol. 89, no. 3, pp. 366–374, 2001.

[7] M. Köhler, “Wet-chemical etching methods,” *Etch. Microsyst. Technol.*, pp. 29–110, 1999.

[8] P. Verdonck, “Plasma etching,” of. microfabricação proj. e construção de CI`s MOS, Swart J.W., Ed., Campinas (São Paulo, Brazil): UNICAMP, Chap 10, p. 1–11, 2006.

[9] D. M. Mattox, *Handbook of Physical Vapor Deposition (PVD) Processing*. Westwood, NJ: Noyes Publications, 1998.

[10] H. O. Pierson, W. A. Publishing, and N. York, *Handbook of Chemical Vapor Deposition (CVD)*, Norwich, NY: Noyes Publications, 1999.

[11] A. Moridi, S. M. Hassani-Gangaraj, M. Guagliano, and M. Dao, “Cold spray coating: Review of material systems and future perspectives,” *Surf. Eng.*, vol. 30, no. 6, pp. 369–395, 2014.

[12] R. N. Raoelison, C. Verdy, and H. Liao, “Cold gas dynamic spray additive manufacturing today: Deposit possibilities, technological solutions and viable applications,” *Mater. Des.*, vol. 133, pp. 266–287, 2017.

[13] D.-Y. Kim *et al.*, “Cold spray deposition of copper electrodes on silicon and glass substrates,” *J. Therm. Spray Technol.*, vol. 22, no. 7, pp. 1092–1102, 2013.

[14] S. M. Hassani-Gangaraj, A. Moridi, and M. Guagliano, “Critical review of corrosion protection by cold spray coatings,” *Surf. Eng.*, vol. 31, no. 11, pp. 803–815, 2015.

[15] V. K. Champagne, B. Gabriel, and J. Villafuerte, *15 - Cold Spray Coatings to Improve the Corrosion Resistance of Magnesium (Mg) Alloys*. Philadelphia: Woodhead, 2013.

[16] K. B. Perez and C. B. Williams, “Combining additive manufacturing and direct write for integrated electronics – A review,” *Int. Solid free. Fabr. Symp. Proc.*, pp. 962–979, 2013.

[17] P. Richer, M. Yandouzi, L. Beauvais, and B. Jodoin, “Oxidation behaviour of CoNiCrAlY bond coats produced by plasma, HVOF and cold gas dynamic spraying,” *Surf. Coatings Technol.*, vol. 204, no. 24, pp. 3962–3974, 2010.

[18] W. R. Chen, E. Irissou, X. Wu, J. G. Legoux, and B. R. Marple, “The oxidation behavior of TBC with cold spray CoNiCrAlY bond coat,” in *Journal of Thermal Spray Technology*, 2011, vol. 20, no. 1–2, pp. 132–138.

[19] B. S. DeForce, T. J. Eden, and J. K. Potter, “Cold spray Al-5% Mg coatings for the corrosion protection of magnesium alloys,” *J. Therm. Spray Technol.*, vol. 20, no. 6, pp. 1352–1358, 2011.

[20] D. J. Park, H. G. Kim, Y. Il Jung, J. H. Park, J. H. Yang, and Y. H. Koo, “Behavior of an improved Zr fuel cladding with oxidation resistant coating under loss-of-coolant accident conditions,” *J. Nucl. Mater.*, vol. 482, pp. 75–82, 2016.

[21] N. Matthews, “Cold spray applications for the australian defence department,” in: *Int. Therm. Spray Conf. Expo.2012*, 2012.

[22] A. Sova, S. Grigoriev, A. Okunkova, and I. Smurov, “Potential of cold gas dynamic spray as additive manufacturing technology,” *Int. J. Adv. Manuf. Technol.*, vol. 69, no. 9–12, pp. 2269–2278, 2013.

[23] M. E. Lynch *et al.*, “Design and topology/shape structural optimisation for additively manufactured cold sprayed components,” *Virtual Phys. Prototyp.*, vol. 8, no. 3, pp. 213–231, 2013.

[24] P. F. Leyman and V. K. Champagne, “Cold spray process development for the reclamation of the Apache helicopter mast support,” Army Research Laboratory, Aberdeen Proving Ground, MD, Tech. Rep. ARL-TR-4922, 2009.

[25] K. Tamai, K. Kawate, I. Kawahara, Y. Takakura, and K. Sakaki, “Inorganic antimicrobial coating for titanium alloy and its effect on bacteria,” *J. Orthop. Sci.*, vol. 14, no. 2, pp. 204–209, 2009.

[26] S. V. Klinkov, V. F. Kosarev, N. S. Ryashin, and V. S. Shikalov, “Experimental study of cold gas spraying through a mask. Part 1,” *Thermophys. Aeromechanics*, vol. 23, no. 5, pp. 735–740, 2016.

[27] Y. Cormier, P. Dupuis, B. Jodoin, and A. Corbeil, “Net shape fins for compact heat exchanger produced by cold spray,” *J. Therm. Spray Technol.*, vol. 22, no. 7, pp. 1210–1221, 2013.

[28] P. Dupuis, Y. Cormier, A. Farjam, B. Jodoin, and A. Corbeil, “Performance evaluation of near-net pyramidal shaped fin arrays manufactured by cold spray,” *Int. J. Heat Mass Transf.*, vol. 69, pp. 34–43, 2014.

[29] Y. Cormier, P. Dupuis, A. Farjam, A. Corbeil, and B. Jodoin, “Additive manufacturing of pyramidal pin fins: Height and fin density effects under forced convection,” *Int. J. Heat Mass Transf.*, vol. 75, pp. 235–244, 2014.

[30] T. Schmidt, F. Gärtner, H. Assadi, and H. Kreye, “Development of a generalized parameter window for cold spray deposition,” *Acta Mater.*, vol. 54, no. 3, pp. 729–742, 2006.

[31] R. C. Dykhuizen and M. F. Smith, “Gas dynamic principles of cold spray,” *J. Therm. Spray Technol.*, vol. 7, no. 2, pp. 205–212, 1998.

[32] F. Gärtner, T. Stoltenhoff, T. Schmidt, and H. Kreye, “The cold spray process and its potential for industrial applications,” *J. Therm. Spray Technol.*, vol. 15, no. 2, pp. 223–232, 2006.

[33] H. Assadi, F. Gärtner, T. Stoltenhoff, and H. Kreye, “Bonding mechanism in cold gas spraying,” *Acta Mater.*, vol. 51, no. 15, pp. 4379–4394, 2003.

[34] T. Stoltenhoff, H. Kreye, and H. J. Richter, “An analysis of the cold spray process and its coatings,” *J. Therm. Spray Technol.*, vol. 11, no. 4, pp. 542–550, 2002.

[35] M. F. Smith, “Comparing cold spray with thermal spray coating technologies,” in *The Cold Spray Materials Deposition Process: Fundamentals and Applications,* V.K Champagne, Ed., Boca Raton, FL: Woodhead, 2007.

[36] J. Villafuerte and D. Wright, “Practical cold spray success: Repair of Al and Mg alloy aircraft components,” *Adv. Mater. Process.*, vol. 168, no. 5, pp. 53–55, 2010.

[37] M. Grujicic, C. L. Zhao, W. S. DeRosset, and D. Helfritch, “Adiabatic shear instability based mechanism for particles/substrate bonding in the cold-gas dynamic-spray process,” *Mater. Des.*, vol. 25, no. 8, pp. 681–688, 2004.

[38] M. Grujicic, J. R. Saylor, D. E. Beasley, W. S. DeRosset, and D. Helfritch, “Computational analysis of the interfacial bonding between feed-powder particles and the substrate in the cold-gas dynamic-spray process,” *Appl. Surf. Sci.*, vol. 219, no. 3–4, pp. 211–227, 2003.

[39] J. Pattison, S. Celotto, A. Khan, and W. O’Neill, “Standoff distance and bow shock phenomena in the Cold Spray process,” *Surf. Coatings Technol.*, vol. 202, no. 8, pp. 1443–1454, 2008.

[40] V. K. Champagne, D. Helfritch, P. Leyman, S. Grendahl, and B. Klotz, “Interface material mixing formed by the deposition of Copper on Aluminum by means of the cold spray process,” *J. Therm. Spray Technol.*, vol. 14, no. 3, pp. 330–334, 2005.

[41] R. Ghelichi and M. Guagliano, “Coating by the cold spray process: a state of the art,” *Frat. ed Integrità Strutt.*, vol. 8, pp. 30–44, 2009.

[42] X. J. Ning, J. H. Jang, and H. J. Kim, “The effects of powder properties on in-flight particle velocity and deposition process during low pressure cold spray process,” *Appl. Surf. Sci.*, vol. 253, no. 18, pp. 7449–7455, 2007.

[43] Y. Cormier, P. Dupuis, B. Jodoin, and A. Corbeil, “Mechanical properties of cold gas dynamic-sprayed near-net-shaped fin arrays,” *J. Therm. Spray Technol.*, vol. 24, no. 3, pp. 476–488, 2014.

[44] A. Sova, M. Doubenskaia, S. Grigoriev, A. Okunkova, and I. Smurov, “Parameters of the gas-powder supersonic jet in cold spraying using a mask,” *J. Therm. Spray Technol.*, vol. 22, no. 4, pp. 551–556, 2013.

[45] T. Van Steenkiste and J. R. Smith, “Evaluation of coatings produced via kinetic and cold spray processes,” *J. Therm. Spray Technol.*, vol. 13, no. 2, pp. 274–282, 2004.

[46] T. Z. Blazynski, *Explosive Welding, Forming and Compaction*. London: Applied Science Publishers, 1983.

THIS PAGE INTENTIONALLY LEFT BLANK

INITIAL DISTRIBUTION LIST

1. Defense Technical Information Center
   Ft. Belvoir, Virginia

2. Dudley Knox Library
   Naval Postgraduate School
   Monterey, California

.